

# Sea quark effects in $B$ Spectroscopy and Decay Constants

S. Collins\*

*Deutsches Elektron-Synchrotron DESY, D-15735 Zeuthen, Germany*

C. T. H. Davies†

*University of Glasgow, Glasgow, Scotland G12 8QQ*

U. M. Heller

*SCRI, Florida State University, Tallahassee, Fl 32306-4052, USA*

A. Ali Khan‡ and J. Shigemitsu

*The Ohio State University, Columbus, Ohio 43210, USA*

J. Sloan

*University of Kentucky, Lexington, KY 40506-0055, USA*

C. Morningstar

*University of California at San Diego, La Jolla, CA 92093, USA*

## Abstract

We present comprehensive results for the spectrum and decay constants of hadrons containing a single  $b$  quark. The heavy quark is simulated using an  $O(1/M)$  NRQCD action and the light quark using the  $O(a)$  tadpole-improved clover action on gauge configurations containing two degenerate flavours of sea quarks at  $\beta^{n_f=2} = 5.6$  provided by the HEMCGC collaboration. We present detailed results for the lower lying  $S$  and  $P$  wave  $B$  meson states and the  $\Lambda_b$  baryon. We find broad agreement

---

\*On leave of absence from the University of Glasgow.

†UKQCD Collaboration.

‡Present address: Center for Computational Physics, University of Tsukuba, Ibaraki 305-8577, Japan.

with experiment. In addition, we present results for the pseudoscalar and, for the first time, the vector decay constants fully consistent to  $O(\alpha/M)$ :  $f_B = 186(5)(stat)(19)(pert)(9)(disc)(13)(NRQCD)(+50)(a^{-1})$  MeV,  $f_B^* = 181(6)(stat)(18)(pert)(9)(disc)(13)(NRQCD)(+55)(a^{-1})$  MeV and  $f_{B_s}/f_B = 1.14(2)(stat)(-2)(\kappa_s)$ . We present an investigation of sea quark effects in the  $B$  spectrum and decay constants. We compare our results with those from similar quenched simulations at  $\beta^{n_f=0} = 6.0$ . For the spectrum, the quenched results reproduce the experimental spectrum well and there is no significant difference between the quenched and  $n_f = 2$  results. For the decay constants, our results suggest that sea quark effects may be large.

## I. INTRODUCTION

Hadrons containing a single  $b$  quark hold the key to many important questions facing particle physics. In particular, the weak decays of these particles are being studied to look for inconsistencies in the Standard Model and indications of new physics beyond it. Lattice calculations have a central and fundamental role to play in this pursuit. Not only is lattice theory a first principles approach but also offers the most reliable way to calculate the masses of heavy-light hadrons and the low-energy QCD factors which are needed to extract the electroweak physics from experiment. An introduction to  $B$  physics and the theoretical advances in this field, for example Heavy Quark Effective Theory (HQET), as well as the contribution made from lattice theory, can be found in reference [1].

The aim of a lattice calculation of  $B$  meson phenomenology is to produce reliable predictions where the systematic errors, such as finite lattice spacing, finite volume and quenching, are understood and under control. Our approach is to systematically improve the actions used for the heavy and light quark and to use lattices with physical volumes large enough to accommodate at least the lower lying  $B$  mesons. In particular, we simulate the  $b$  quark on the lattice using NRQCD: a cut-off of the order of the heavy mass is imposed and we cannot extrapolate to the continuum. This requires the systematic errors to be reduced to the order of the statistical errors at finite  $\beta$ . In this paper, we argue that the uncertainty arising from finite  $a$ , volume, and the truncation of the NRQCD series are under control and it is now reasonable to investigate the effects of quenching. As a first step towards predicting  $B$ -meson properties in full QCD, we perform a simulation of the  $B$  spectrum and decay constants including two degenerate flavours of dynamical quarks. We then make a comparison with our previous NRQCD calculations on quenched configurations [2,3] and study the sensitivity of various quantities to the presence of sea quarks.

The paper is organised as follows: in the next section we describe the details of the simulation. Each choice of quark action and simulation parameter leads to an associated systematic error and the corresponding effect on predictions for the  $B$  spectrum and decay constants are discussed in section III. Results for the spectrum are presented in section IV and compared with experiment. We then study the effect of sea quarks on the  $B$  spectrum and  $\Lambda_b$  in section IV A.

The next section deals with the pseudoscalar and vector decay constants. The lattice operators required to compute the decay constants to  $O(1/M)$  and the corresponding 1-loop

perturbative matching factors are introduced and discussed. In addition, the expectations from Heavy Quark Symmetry (HQS) for the heavy quark mass dependence of these quantities is outlined. Our results for  $f_B$ ,  $f_{B_s}$ ,  $f_{B^*}$  and  $f_{B_s^*}$  are presented in section V A and their dependence on the heavy quark mass is investigated. Finally, we present a detailed study of sea quarks effects in the decay constants.

## II. SIMULATION DETAILS

The simulations were performed using  $100 \ 16^3 \times 32$  gauge configurations at  $\beta = 5.6$  with two flavours of staggered dynamical sea quarks with a bare quark mass of  $am_{sea} = 0.01$ , which roughly corresponds to  $m_\pi/m_\rho = 0.525$ . These configurations were generously made available by the HEMCGC collaboration; more details can be found in [4]. We fixed the configurations to the Coulomb gauge.

The light quark propagators were generated using the clover fermion action at three values of the hopping parameter,  $\kappa = 0.1385$ ,  $0.1393$  and  $0.1401$ . From an analysis of the light hadron spectrum [5], the second  $\kappa$  value corresponds to a quark mass close to strange, where  $\kappa_s = 0.1392(1)$  from  $M_K$ ,  $\kappa_s = 0.1394(1)$  from  $M_{K^*}$  and  $0.1392(1)$  from  $M_\phi$ ;  $\kappa_c = 0.1408$ . The  $O(a)$  improvement term in the clover action is implemented with a tadpole-improved value for the clover coefficient,  $c_{sw}$ . This amounts to dividing all the gauge links by  $u_0$ , where we use  $u_0 = 0.867$  measured from the plaquette, and setting the coefficient to the tree-level value  $c_{sw} = 1$ . In order to improve matrix elements to the same order as the spectrum, we use the prescription proposed by the Fermilab group [6] and replace the quark field normalisation  $\sqrt{2\kappa}$  with  $\sqrt{1 - 6\tilde{\kappa}}$ , where  $\tilde{\kappa} = u_0\kappa$ .

In this simulation we truncate the NRQCD series at  $O(1/M_0)$ , where  $M_0$  is the bare heavy quark mass, and the action takes the form:

$$S = \psi^\dagger(D_t + H_0 + \delta H)\psi \quad (1)$$

where

$$H_0 = -\frac{\Delta^{(2)}}{2M_0} \quad \text{and} \quad \delta H = -c_B \frac{\sigma \cdot B}{2M_0}. \quad (2)$$

Tadpole improvement of the gauge links is used throughout and the hyperfine coefficient is given the tree-level value  $c_B = 1$ . We use the standard clover-leaf operator for the  $B$  field. The heavy quark propagators were computed using the evolution equation [7]:

$$G_{t+1} = \left(1 - \frac{a\delta H}{2}\right) \left(1 - \frac{aH_0}{2n}\right)^n U_4^\dagger \left(1 - \frac{aH_0}{2n}\right)^n \left(1 - \frac{a\delta H}{2}\right) G_t \quad (3)$$

for all  $t$ , where  $n$  is the stabilising parameter.

We generated heavy quark propagators at 10 values of  $(aM_0, n)$  corresponding to  $(0.8, 5)$ ,  $(1.0, 4)$ ,  $(1.2, 3)$ ,  $(1.7, 2)$ ,  $(2.0, 2)$ ,  $(3.0, 2)$ ,  $(3.5, 2)$ ,  $(4.0, 2)$ ,  $(7.0, 1)$  and  $(10.0, 1)$ . This roughly corresponds to a range of meson masses from  $M_B/3$  to  $4M_B$  and is sufficient for a reasonable investigation of heavy quark symmetry. Results in the static limit are not presented. We were not able to improve on the quality of the signal compared to previous results using

Wilson light fermions [8,9], and in this case the extrapolation of the NRQCD results to the static limit was considered more reliable than results at the static point itself. To improve statistics we have also calculated the propagators on the time-reversed configurations.

Details of the fitting analysis and extraction of the spectral quantities and decay constants from the heavy-light meson correlators can be found in the appendix.

### III. SYSTEMATIC ERRORS

In this section we discuss the systematic errors associated with our choice of quark actions and simulation parameters. In previous work we used Wilson light fermions which was estimated to introduce the largest systematic error into the calculation of heavy-light quantities. For tadpole-improved clover fermions the systematic errors are now estimated to be a relative error of  $O((a\Lambda_{QCD})^2) \sim 4\%$  (where we take  $a\Lambda_{QCD} = a\Lambda_V = 0.185$  for these configurations) in quantities of  $O(\Lambda_{QCD})$ . However, significant residual  $O(\alpha a\Lambda_{QCD})$  errors may remain in this simulation. An investigation of the scaling behaviour of quenched light hadron masses using a nonperturbative determination of the  $O(a)$  improvement coefficient [10] in the clover action concluded that these errors are negligible for  $\beta^{n_f=0} \gtrsim 6.0$  [11]. The remaining scaling violations at these  $\beta$ 's are estimated to be a few percent [11] in the quenched results. In the present study tadpole-improved clover fermions are used for the valence quarks and staggered fermions for the dynamical quarks (which introduce  $O(\alpha a^2)$  errors). Since  $\beta^{n_f=2} = 5.6$  corresponds to roughly the same lattice spacing as that at  $\beta^{n_f=0} = 6.0$  (see table II) we do not expect the associated scaling violations to be larger than in the quenched case.

The truncation of the NRQCD series at  $O(1/M)$  introduces an absolute error of  $O(\Lambda_{QCD}(\Lambda_{QCD}/M)^2)$ . This corresponds to approximately 1% errors in quantities of  $O(\Lambda_{QCD})$  and 10% errors in the coefficients of the heavy quark expansion at  $M_B$ . In fact the significance of the higher order terms omitted from the action depends on the quantity considered. The additional terms to  $O(1/M^2)$  and the leading  $1/M^3$  terms are:

$$\begin{aligned} \delta H_{h.o.} = & -c_3 \frac{g}{8(M_0)^2} \sigma \cdot (\nabla \times E - E \times \nabla) + c_2 \frac{ig}{8(M_0)^2} (\nabla \cdot E - E \cdot \nabla) \\ & -c_1 \frac{(\Delta^{(2)})^2}{8(M_0)^3} + c_4 \frac{a^2 \Delta^{(4)}}{24M_0} - c_5 \frac{a(\Delta^{(2)})^2}{16n(M_0)^2}, \end{aligned} \quad (4)$$

where  $\nabla$  is the symmetric gauge-covariant lattice derivative and  $\Delta^{(4)}$  is a discretised version of the continuum operator  $\sum D_i^4$ . The first two terms, of  $O(1/M^2)$ , represent the spin-orbit interaction (s.o.) and the Darwin term, respectively. The s.o. interaction only contributes to states with non-zero angular momentum and is a  $1/M^2 \sim 1\%$  correction to the s.o. interaction arising from the light quark, which dominates (see the next section). The Darwin term is a  $\sim 1\%$  spin-independent shift which appears in both  $S$  and  $P$  states, but which does not affect spin splittings, such as the hyperfine splitting. The next order terms at  $O(1/M^3) \sim 0.1\%$  are due to corrections to the kinetic energy and discretisation corrections and should be even less significant. Of course, all the terms in  $\delta H_{h.o.}$  will affect predictions through the change in the meson mass. However, for example the  $1/M^2$  terms represent

a .1% correction to the meson mass, and hence, the shift in the meson mass has a less significant effect on predictions than those already mentioned.

Indeed, a comparison by Ishikawa et al [12] of the low lying  $S$ -state heavy-light spectrum derived from an NRQCD action correct to  $O(1/M)$  and that including the additional terms in equation 4 showed the higher order terms to be insignificant. A more detailed analysis of the effect of higher order terms on the  $S$ -state spectrum has been performed by Lewis and Woloshyn [13]. These authors verified that the importance of the terms in the NRQCD action follows the expectations of naive power counting, i.e.  $|O(1/M^3)| < |O(1/M^2)| < |O(1/M)|$ , where all  $O(1/M^3)$  terms were included. Terms of  $O(1/M^2)$  and  $O(1/M^3)$  were found to have a negligible effect on the  $S$ -state  $B$  meson mass splittings.

Ishikawa et al also compared the results for the pseudoscalar and vector decay constant including tree-level terms to  $O(1/M)$  and  $O(1/M^2)$  (for these quantities, corrections to the currents as well as to the action must be considered). The decay constants differed by approximately 3% at the  $B$  meson, and, 6% is, conservatively, estimated to be the corresponding error in  $f_B$  if  $\delta H_{h.o.}$  and the  $O(1/M^2)$  current corrections are omitted.

An additional uncertainty is introduced through the use of the tree-level value (with tadpole-improvement) for the hyperfine coefficient,  $c_B$ . Tadpole improvement is expected to account for most of the renormalisation of this factor. However, an error of  $O(\alpha\Lambda_{QCD}(\Lambda_{QCD}/M))$  will remain; for example this corresponds to approximately 10–30%, for  $\alpha \sim 0.1–0.3$  in the  $B^*–B$  splitting, which is proportional to  $c_B$ . The one-loop correction to  $c_B$  has been calculated [14] and for  $M_0 = 1.9$ , a bare quark mass close to  $M_0^b$  for this simulation,  $c_B \sim 1.15–1.3$ , depending on the characteristic scale  $q^*$  used.

For the determination of  $f_B$  and  $f_{B^*}$ , the factors matching the lattice currents to the full continuum QCD currents must be calculated. Morningstar and Shigemitsu have computed these factors for both the axial-vector [15] and vector [16] currents. The mixing at  $O(\alpha)$  among heavy-light current operators has been fully taken into account. In addition, an  $O(\alpha(a\Lambda_{QCD}))$  discretisation correction to the current was found and corrected for in the case of clover light fermions. This has been discussed in detail in [3,17], and we present an outline in section V. The largest remaining perturbative error is  $O(\alpha^2) \sim 1–10\%$ .

Combining the tadpole-improved clover action for light quarks with the  $O(1/M^2)$  NRQCD action, Hein et al [18] found no significant scaling violations in results for the quenched  $B$  spectrum and decay constant between  $\beta^{n_f=0} = 6.0$  and 5.7. The results from a recent quenched calculation by Ishikawa et al [19] of  $f_B$  at three  $\beta$  values in the range 5.7–6.1 supports this finding.

A further continuing uncertainty is the possibility of large finite volume effects. A study by Duncan et al [20] in the static limit in the quenched approximation found no significant finite volume effects in the results for the lowest lying  $S$ -state  $B$  mesons (and in particular for  $f_B$ ) for a box size as small as 1.3 fm. Finite volume effects are likely to be larger when dynamical quarks are included [21]. However, since for our simulation,  $L = 1.6$  fm, for a visible effect, finite volume problems would have to be very different in the dynamical case, despite the fairly heavy sea quark masses ( $m_{sea}$  is around the strange quark mass) that we use. A preliminary study by the SESAM collaboration [22], using sea quark masses which correspond to  $m_\pi/m_\rho = 0.69$ , found the finite volume effects for the  $\rho$  meson (which is bigger physically than the lowest lying  $S$ -state  $B$  mesons) to be small, less than 5% for a lattice size similar to that used in this work. However, in the absence of a detailed investigation of

finite volume effects for  $B$  mesons at  $n_f = 2$  this remains an unknown effect.

Table I summarises the systematic errors expected to dominate each mass splitting and combination of decay constants. In general, our statistical errors are of a comparable size. The only significant exception is for the radial and orbital excitations of the  $B$  meson and the  $\Lambda_b$  baryon. These particles are probably squeezed on a box of extent  $1.6fm$ , although for  $B(1P)-B(1S)$  and  $B(2S)-B(1S)$  our statistical errors are also large.

While within the  $B$  system we are close to achieving our goal of controlling the main systematic errors, a major uncertainty is introduced when we convert from lattice numbers to physical predictions. In particular, this uncertainty affects predictions through the fixing of the quark masses (discussed below) as well as the final conversion from lattice units to MeV. Ideally one would fix the lattice spacing using a quantity within the  $B$  system. However, with the exception of the lowest lying  $S$ -states, the experimental results for the  $B$  spectrum are still preliminary and it is unfeasible to fix  $a$ , for example, from the  $P-S$  or  $2S-1S$  splitting (which have little dependence on  $m_Q$ ). Thus, one must consider determinations of  $a$  from light and heavy spectroscopy; table II gives some examples for these configurations.

As in the discussion above for heavy-light hadrons the effect of systematic errors on the value of the lattice spacing must be considered. We computed  $m_\rho$  using the tadpole-improved clover action and results for this quantity from quenched studies are consistent with minimal discretisation errors in this quantity for  $a^{-1} \sim 2$  GeV [11]. Similarly, the  $b\bar{b}$  spectrum was computed with an  $Mv^4$  NRQCD action, and in quenched studies the spin-averaged splittings obtained using this action show no scaling violations in the same range of lattice spacings [23].

Finite volume effects may affect  $m_\rho$  for a box size of  $(1.6\text{ fm})^3$  (this is not expected to be an issue for heavy quarkonia). These effects are not thought to be significant for a calculation of  $m_\rho$  with similar parameters in the quenched approximation (such as that detailed in table II) [24]. However, finite volume problems are expected to be larger when dynamical quarks are introduced [21]. Naively, one expects  $m_\rho$  to be overestimated, and hence  $a^{-1}$  underestimated if the meson is squeezed on a finite lattice. Although the preliminary SESAM study, mentioned above, suggests this may not be significant, finite volume dependence remains an uncertainty.

Table II indicates there is a large discrepancy between  $a^{-1}$  determined from light and heavy spectroscopy for the HEMCGC configurations. In the quenched approximation, different lattice spacings are expected from quantities dominated by different physical scales and one must choose the most relevant quantity with which to fix  $a$ . When dynamical quarks are partially introduced some convergence in the estimates of  $a^{-1}$  is expected (although with  $m_{sea} \sim m_{strange}$  significant residual quenching effects will probably remain) and the choice of quantity to determine  $a$  should be less important. However, the range in  $a^{-1}$  is comparable to that seen in the quenched approximation at  $\beta^{n_f=0} = 6.0$ , also detailed in the table (the same light quark and NRQCD actions were employed);  $1P-1S/m_\rho = .43(1)$  and  $.46(1)$  for  $n_f = 0$  and 2 respectively, compared to 0.57 from experiment. One possibility is that introducing two flavours of sea quarks with  $m_{sea} \sim m_{strange}$  produces little effect on  $m_\rho/\Upsilon(1P-1S)$ . Alternatively, any effect of the sea quarks may be counteracted by more significant finite volume problems (or some other systematic error dependent on the number of sea quarks) at  $n_f = 2$  for  $m_\rho$  compared to  $n_f = 0$ .

Until this issue has been clarified, we choose the lattice spacing from  $m_\rho$  to convert to

physical units at  $n_f = 2$  and use  $a^{-1} = 2.4$  GeV to give a (conservative) indication of the uncertainty in  $a^{-1}$ . This translates into an error in physical predictions at least as large as those already mentioned. We comment on how to compare our results for heavy-light hadrons with those from quenched simulations below.

To pin-point the  $B$  and  $B_s$  mesons from the range of meson masses simulated in this study we must fix the bare quark masses corresponding to the lightest quark ( $u, d$ ), the strange quark and the bottom quark. The bare mass of the lightest quark is fixed in the standard way by extrapolating the pion mass to zero. As indicated above,  $m_s^0$  is derived from the  $\phi$ ,  $K$  and  $K^*$  mesons, and we use the difference in the results as an estimate of the uncertainty in  $\kappa_s$ . The magnitude of this error found in the  $B_s$ – $B$  splitting and the ratio  $f_B/f_{B_s}$  is given in table I. In order to determine  $M_b^0$  we must first correct the meson simulation energies for the removal of the mass term in the NRQCD action. As detailed in [8] we use the mass shift calculated from heavy quarkonia dispersion behaviour to obtain the heavy-light meson masses from the simulation energies. Thus, interpolating between our results for the pseudoscalar meson until we obtain the  $B$  meson mass, we find  $aM_b^0 = 2.1$ – $1.8$  for  $a^{-1} = 2.0$ – $2.4$  GeV.

In order to investigate sea quark effects we need to compare our results with similar calculations in the quenched approximation. While we believe the dominant systematic errors are under control, most of the remaining residual uncertainties are minimised if we compare with a simulation which uses a lattice with a similar lattice spacing and physical volume. From table II  $\beta = 6.0$  in the quenched approximation roughly matches  $\beta = 5.6$  at  $n_f = 2$ . References [3] and [2] report on NRQCD results using tadpole-improved clover light quarks at this  $\beta$ , on a lattice volume of  $\sim (1.6fm)^3$ . A higher-order NRQCD action is employed for the heavy quarks ( $H_{h.o.}$  is included), however, considering the negligible effect these terms have at the  $B$  meson mass, these quenched results are suitable for comparison.

For the quenched simulation the lattice spacing derived from light spectroscopy is considered most relevant for  $B$  splittings and decay constants which are expected to be dominated by the ‘brown muck’. Thus, we initially compare the two simulations fixing the lattice spacing from  $m_\rho$  in both cases. The effect on the comparison of the large uncertainty in  $a^{-1}$  for  $n_f = 2$  is also considered.

Within our study it is premature to attempt an extrapolation of the quenched and unquenched data to a physically relevant number of sea quark flavours. We introduce uncertainties by implementing clover light valence fermions while using staggered sea fermions. In addition, we chirally extrapolate the valence light quarks to zero light quark mass while keeping the sea quark mass fixed around the strange quark mass. Thus, our simulation does not correspond to that for a light and heavy quark bound state with a sea of two flavours of physical quarks. However, inserting dynamical quarks allows the sensitivity of various quantities to these effects to be investigated. A more systematic approach to sea quark effects is reserved for later work.

#### IV. SPECTRUM RESULTS

Figure 1 presents our results for the lower lying  $B$  meson spectrum and the  $\Lambda_b$  baryon compared to experiment. At this initial stage our results are in broad agreement with

experiment. The experimental results for all but the lowest states are still uncertain. In particular, there are only preliminary signals for the  $2S$  and  $P$  states. For the latter, a signal has been found for a  $B\pi\pi$  resonance [25], which is probably has  $j_l = 3/2$ , and a  $B^{(*)}\pi$  resonance [26], which is likely to be a superposition of various  $P$  states. Our result for the  $P$  state ( $B_1^*$ ) is obtained from an operator with quantum numbers  $^1P_1$  in the  $^{2S+1}L_J$  nomenclature of quarkonia. Since charge conjugation is not a symmetry in the heavy-light system the two  $l = 1$ ,  $J = 1$  states mix and thus our operator has an overlap with both states. We investigated this mixing by forming a matrix of correlators with the  $^3P_1$  operator. However, these operators were found to be degenerate at this level of statistics. In fact, we are unable to resolve any splitting between the  $P$  states in this study.

In addition, we can compare with the theoretical expectations from Heavy Quark Symmetry (HQS), shown in figure 2 [27]. The picture of a heavy quark surrounded by a light quark cloud, where the heavy quark acts merely as a colour source in the heavy quark limit, predicts a gross spectrum determined by the light quark degrees of freedom; this gives rise to meson mass splittings of  $O(\Lambda_{QCD})$  which are independent of the heavy quark at lowest order. In particular, the large scale features of the spectrum are due to the radial ( $2S$ ) and orbital ( $1P$ ) excitation of the light quark. At the next order are the  $j_l = 3/2$  and  $1/2$  doublets of the  $P$  states, which are split due to the spin-orbit interaction. The  $2S-1S$  and  $P-S$  splittings in figure 1 are 300–600 MeV or  $O(\Lambda_{QCD})$ , in agreement with this naive picture. Similarly, heavy-light hadrons which only differ from the  $B$  meson in the light quark flavour, for example  $B_s$ , or the number of light quarks, for example  $\Lambda_b$ , will also give rise to splittings independent of  $m_Q$  at lowest order.

At finite  $m_Q$ , flavour and spin symmetry are broken by the kinetic energy of the heavy quark and the hyperfine interaction. The latter removes the degeneracy in the heavy quark spin, for example in the  $j_l = 1/2$  S-states and the  $j_l = 3/2$  and  $j_l = 1/2$  P-states. These hyperfine doublets are expected to be split by  $O(\Lambda_{QCD}^2/M) \sim 50$  MeV; this compares well with the experimental hyperfine splitting,  $B^*-B = 46$  MeV. These splittings vanish as  $1/M$  in the static limit.

Our results are compared with experiment in more detail, taking into account the systematic errors, in table III. If we assume, initially,  $a^{-1} = 2.0$  GeV is a reasonable estimate of the lattice spacing for these configurations the only significant disagreement with experiment is found in the  $\Lambda_b-B$  splitting. Finite volume effects, which are not included in the estimates of the systematic errors, may well account for the rather high value for the  $\Lambda_b$  mass. For all splittings, the error from setting  $a^{-1}$  is at least as large as the statistical or other systematic errors. However, since this uncertainty leads to a positive shift in the splittings it does not lessen the disagreement with experiment found for the  $\Lambda_b-B$  splitting. There is also less agreement for the  $B_s-B$  and  $B^{**}-B$  splittings using  $a^{-1} = 2.4$  GeV.

With the mass splittings calculated for a wide range of heavy quark masses, not just in the region of the  $B$  meson, we are able to investigate violations of HQS at finite  $m_Q$ . The behaviour of these splittings as a function of  $1/M_{PS}$  is shown in figures 3 and 4, in lattice units. The  $\bar{E}(2S)-\bar{E}(1S)$ ,  $E(^1S_0)_{\kappa_s}-E(^1S_0)_{\kappa_d}$ ,  $E(\Lambda_Q)-\bar{E}(1S)$  and  $E(^1P_1)-\bar{E}(1S)$  splittings are very weakly (and linearly) dependent on  $1/m_Q$ , consistent with behaviour dominated by the light quark, with small corrections due to the kinetic energy of the heavy quark and the hyperfine interaction;  $E(^1S_0)$  denotes the simulation energy of a pseudoscalar meson, while  $\bar{E}(1S)$  denotes the spin-average of the simulation energy with the corresponding



vector meson.  $E(^1S_0)_{\kappa_s}$  indicates that the light quark mass has been interpolated to that of the strange quark mass. Note that by taking the spin-average the dependence of that mass on the hyperfine term is removed. Similarly, the hyperfine splitting in the  $1S$  and  $2S$  states depends linearly on  $1/m_Q$  over the range of masses studied, vanishing in the static limit, as expected theoretically.

To quantify the heavy quark mass dependence we fit the mass splittings to the form:

$$\Delta M = C_0 + C_1/M + \dots \quad (5)$$

where  $M$  is the pseudoscalar meson mass, and extract the coefficients  $C_0$  and  $C_1$ , which are expected to be of  $O(\Lambda_{QCD})$  and  $O(\Lambda_{QCD}^2)$  respectively (with the exception of the hyperfine splittings where  $C_0 = 0$ ). In fact, the coefficients can be related to the binding energy and expectation values of the kinetic energy of the heavy quark and the hyperfine interaction in the static limit for each meson or baryon. These quantities are needed in analytical approaches such as HQET.

If we define the heavy-light hadron binding energy,  $\bar{\Lambda}_H^{m_Q}$ , using:

$$M_H = m_Q + \bar{\Lambda}_H^{m_Q} \quad (6)$$

where  $M_H$  is the mass of the hadron, and expand using first order perturbation theory,

$$\bar{\Lambda}_H^{m_Q} = \bar{\Lambda}_H + \frac{1}{M} \langle H | \mathcal{O}_{kin} | H \rangle + \frac{1}{M} \langle H | \mathcal{O}_{hyp} | H \rangle \quad (7)$$

where  $\langle H |$  and  $\bar{\Lambda}_H$  represent the hadron state and the binding energy, respectively, in the infinite mass limit;  $\mathcal{O}_{kin} = -\psi^\dagger(D^2/2)\psi$  and  $\mathcal{O}_{hyp} = -\psi^\dagger(\sigma \cdot B/2)\psi$ . In principle, the separation of the meson mass into the heavy quark mass and binding energy in equation 6 must be clearly defined. However, we only consider physical mass splittings, for which the differences in the definitions of  $\bar{\Lambda}_H^{m_Q}$  cancel. This has the additional benefit that the  $O(1/M)$  coefficients of the mass splittings correspond to the physical difference in expectation values of the kinetic energy (and/or hyperfine interaction) of the particles in the splitting. Thus, we consider, for example, the  $2S-1S$  mass splitting of the spin-average S-states, which can be expressed as

$$\bar{E}(2S) - \bar{E}(1S) = \bar{\Lambda}_{2S} - \bar{\Lambda}_{1S} + \frac{1}{M} \langle 2S | \mathcal{O}_{kin} | 2S \rangle_{phys} - \frac{1}{M} \langle 1S | \mathcal{O}_{kin} | 1S \rangle_{phys} \quad (8)$$

where  $\langle 1S | \mathcal{O}_{kin} | 1S \rangle_{phys}$  denotes the physical expectation value of the kinetic energy in the  $B$  meson. The results are given in table IV in physical units and compared with the theoretical expectation.

Given the weak dependence of most splittings on the heavy quark mass, an estimate of the intercept and slope for some splittings can be made from the experimental results for the  $B$  and  $D$  spectrum and  $\Lambda_b$  and  $\Lambda_c$  baryons. The hyperfine splittings are strongly dependent on  $m_Q$ . However, the intercept is zero, and this can be used along with the splitting for the  $B$  meson to estimate the slope. The corresponding estimates of the intercept and slope of various meson and baryon mass splittings are also shown in the table.

Table IV shows that for quantities which are weakly dependent on  $1/m_Q$ , we can reliably extract  $C_0$ . However, it is difficult to reliably extract the slope and an increase in statistics

is required in order to provide quantitative predictions. Qualitatively, the results are consistent with the theoretical predictions of only small violations of HQS,  $O(\Lambda_{QCD}/M) \sim 10\%$ , around the  $B$  meson. Comparing with the estimates derived from experiment we find our value for the slope of the hyperfine splitting is low, reflecting the low value we obtain for the  $B^*-B$  splitting. The absolute statistical error in the splitting is more or less constant with  $m_Q$ , while the splitting rises as the mass decreases. Thus, a low value of the slope is a clearer indication than the  $B$  hyperfine splitting itself, that our results are inconsistent with experiment. The hyperfine coefficient,  $c_B$ , depends on the heavy quark mass and a determination of this coefficient for the range of masses studied here is needed to clarify the source of any remaining discrepancy with experiment, for example residual quenching effects. Reasonable agreement is found between the lattice results for the  $E(^1S_0)_{\kappa_s} - E(^1S_0)_{\kappa_d}$  splitting and the estimates from experiment. This is also the case for the slope of the  $E(\Lambda_b) - \bar{E}(1S)$  splitting, while the intercept is too high (consistent with finite volume problems mentioned previously). Our results for the intercepts and slopes of spectral quantities are consistent with our previous estimates using Wilson light quarks detailed in reference [8].

### A. $n_f$ dependence

An indication of sea quark effects can be found by comparing the  $n_f = 2$  results with our previous spectrum calculation in the quenched approximation at  $\beta = 6.0$ , detailed in reference [2]. The results for the splittings which have been calculated in both cases are detailed in figure 1 and table V, where  $a^{-1}$  is fixed from  $m_\rho$  in both cases. With the exception of the hyperfine splitting, the quenched simulation reproduces the experimental spectrum well to this level of statistical and systematic uncertainty. Furthermore, comparing with the  $n_f = 2$  results, we see consistency to within  $1-2\sigma$ . However, switching to  $a^{-1} = 2.4$  GeV for the dynamical configurations, differences of  $\sim 3\sigma$  appear for the  $B_s - B$ ,  $B^{**} - B$  and  $\Lambda_b - B$  splittings. The uncertainty in the lattice spacing must be reduced before any clear indications of sea quark effects can be found.

The hyperfine splitting is a quantity where sea quark effects are expected to be seen. However, in practice this is not easy to investigate due to the difficulty in measuring such a small quantity. The quenched results for  $B^* - B$  and  $B_s^* - B_s$ , with lower statistical errors than at  $n_f = 2$ , are approximately half the experimental values. The splittings may be boosted by as much as 30% to  $\sim 31$  and  $\sim 35$  MeV respectively when the 1-loop corrections to  $c_B$  are included. The statistical errors for  $B_s^* - B_s$  are small enough that the splitting is still significantly below experiment, suggesting quenching effects. The corresponding  $n_f = 2$  result is also increased to  $\sim 34$  MeV (for  $a^{-1} = 2.0$  GeV), when  $c_B$  is corrected. However, the statistical error is large and must be reduced significantly before we can see if partially including dynamical quarks increases the hyperfine splitting. Using  $a^{-1} = 2.4$  GeV for the  $n_f = 2$  results only leads to a  $1\sigma$  difference between quenched and  $n_f = 2$  and thus does not significantly change the comparison.

## V. DECAY CONSTANTS

In the continuum, the pseudoscalar (PS) and vector (V) decay constants are defined by

$$\langle 0 | A_0 | PS \rangle = \langle 0 | \bar{q} \gamma_5 \gamma_0 h | PS \rangle = f_{PS} M_{PS}, \quad (9)$$

$$\langle 0 | V_k | V_k \rangle = \langle 0 | \bar{q} \gamma_k h | V_k \rangle = \epsilon_k f_V M_V, \quad (10)$$

where  $q$  and  $h$  represent 4-component light and heavy quark fields respectively. In lattice NRQCD,  $A_0$  and  $V_i$  are given by power series of operators in  $1/M$ . To a given order, all operators with the appropriate quantum numbers and power of  $1/M$  appear. This includes operators representing discretisation corrections, which vanish in the continuum. The corresponding matrix elements for these operators are combined with the renormalisation factors matching the lattice matrix elements to  $\langle 0 | A_0 | PS \rangle$  and  $\langle 0 | V_k | V \rangle$  in full QCD, where mixing between the operators under renormalisation must be taken into account.

In this study we truncate the NRQCD action at  $O(1/M)$ , and match the decay constants to full QCD through  $O(\alpha/M)$ . The axial-vector current is then <sup>1</sup>:

$$\langle A_0 \rangle = \sum_{j=0}^2 C_j(\alpha, aM) \langle J_L^{(j)} \rangle + O(1/M^2, \alpha^2, a^2, \alpha a/M), \quad (11)$$

where

$$\langle J_L^{(0)} \rangle = \langle 0 | \bar{q} \gamma_5 \gamma_0 Q | PS \rangle, \quad (12)$$

$$\langle J_L^{(1)} \rangle = \langle 0 | -\bar{q} \gamma_5 \gamma_0 \frac{\vec{\gamma} \cdot \vec{D}}{2M_0} Q | PS \rangle, \quad (13)$$

$$\langle J_L^{(2)} \rangle = \langle 0 | \bar{q} \frac{\overleftarrow{D} \cdot \overleftarrow{\gamma}}{2M_0} \gamma_5 \gamma_0 Q | PS \rangle. \quad (14)$$

$q$  is now the light quark field in the lattice theory, and  $Q$  is related to the 2-component heavy quark field  $\psi$  in lattice NRQCD by

$$Q = \begin{pmatrix} \psi \\ 0 \end{pmatrix}. \quad (15)$$

$J_L^{(0)}$  and  $J_L^{(1)}$  are the tree-level operators which are obtained through the  $O(1/M)$  inverse Foldy-Wouthuysen transformation connecting  $h$  to  $Q$ .  $J_L^{(2)}$  appears at 1-loop in perturbation theory. Thus,  $C_0$  and  $C_1$  are  $O(1)$ ,

$$C_0 = 1 + \alpha \rho_0, \quad C_1 = 1 + \alpha \rho_1, \quad (16)$$

while  $C_2$  is  $O(\alpha)$ ,

$$C_2 = \alpha(\rho_2 - \zeta_A), \quad (17)$$

where we use the nomenclature of reference [15]. At this order one must also consider an  $O(\alpha a)$  lattice artifact, which appears through the mixing between  $J_A^{(0)}$  and  $J_A^{(2)}$  and which does not vanish in the infinite heavy quark mass limit [15]:

---

<sup>1</sup>In the limit of zero light quark mass.

$$\langle J_L^{disc} \rangle = \langle 0 | a\bar{q} \overleftarrow{D} \cdot \overleftarrow{\gamma} \gamma_5 \gamma_0 Q | PS \rangle. \quad (18)$$

This factor can be viewed as a discretisation correction to  $J_L^{(0)}$ , and hence, we define an improved operator [15]:

$$J_L^{(0)imp} = J_L^{(0)} + C_A J_L^{disc}. \quad (19)$$

where  $C_A = \alpha(1 + \zeta_A/(2aM_0))$ .  $\zeta_A$  reflects the freedom in the definition of the improved operator and is cancelled by the term  $-\alpha\zeta_A$  appearing in  $C_2$ . In practice we set it to zero, which one is free to do at 1-loop accuracy.

In the lattice simulation, the number of matrix elements that must be calculated can be reduced by noting that

$$\frac{1}{2M_0} J_L^{(disc)} = J_L^{(2)}, \quad (20)$$

and, also, that at zero momentum on the lattice

$$\langle J_L^{(1)} \rangle = \langle J_L^{(2)} \rangle. \quad (21)$$

Thus, it is sufficient to compute the matrix elements corresponding to the tree-level operators. Since these matrix elements are generated separately, the contribution to the decay constant from each matrix element in equation 11 can be analysed. For this purpose, we define,

$$f_{PS}^{(j)} \sqrt{M_{PS}} = \frac{1}{\sqrt{M_{PS}}} \langle 0 | J_L^{(j)} | PS \rangle. \quad (22)$$

We use  $f_{PS} \sqrt{M_{PS}}$  to denote the total decay constant at both tree-level and 1-loop.

For the vector current:

$$\langle V_k \rangle = \sum_{j=0}^4 C_{Vj}(\alpha, aM) \langle J_k^{(j)} \rangle + O(1/M^2, \alpha^2, a^2, \alpha a/M) \quad (23)$$

where,

$$\langle J_k^{(0)} \rangle = \langle 0 | \bar{q} \gamma_k Q | V_k \rangle, \quad (24)$$

$$\langle J_k^{(1)} \rangle = \langle 0 | -\bar{q} \gamma_k \frac{\vec{\gamma} \cdot \vec{D}}{2M_0} Q | V_k \rangle, \quad (25)$$

$$\langle J_k^{(2)} \rangle = \langle 0 | -\bar{q} \frac{\overleftarrow{D} \cdot \overleftarrow{\gamma}}{2M_0} \gamma_0 \gamma_k Q | V_k \rangle, \quad (26)$$

$$\langle J_k^{(3)} \rangle = \langle 0 | -\bar{q} \frac{\vec{D}_k}{2M_0} Q | V_k \rangle, \quad (27)$$

$$\langle J_k^{(4)} \rangle = \langle 0 | \bar{q} \frac{\overleftarrow{D}_k}{2M_0} Q | V_k \rangle. \quad (28)$$

$J_k^{(0)}$  and  $J_k^{(1)}$  correspond to tree-level operators, while the rest appear at one-loop in perturbation theory;  $C_{V0}$  and  $C_{V1}$  are  $O(1)$ ,

$$C_{V0} = 1 + \alpha\rho_0^V, \quad C_{V1} = 1 + \alpha\rho_1^V, \quad (29)$$

while  $C_{V2}$ ,  $C_{V3}$  and  $C_{V4}$  are  $O(\alpha)$ ,

$$C_{V2} = \alpha(\rho_2^V - \zeta_V), \quad C_{V3} = \alpha\rho_3^V, \quad C_{V4} = \alpha\rho_4^V. \quad (30)$$

Analogous to the axial-vector case, there is a discretisation correction which can be absorbed into a redefinition of the zeroth order operator:

$$\langle J_k^{disc} \rangle = \langle 0 | -a\bar{q} \overleftarrow{D} \cdot \overleftarrow{\gamma} \gamma_0 \gamma_k Q | V_k \rangle. \quad (31)$$

$$J_k^{(0)imp} = J_k^{(0)} + C_V J_k^{disc}, \quad (32)$$

where  $C_V = \alpha(1 + \zeta_V/(2aM_0))$ ; we set  $\zeta_V = 0$  when computing  $C_V$  and  $C_{V2}$ . Note that,

$$J_k^{(2)} = -J_k^{(1)} + 2J_k^{(3)}, \quad (33)$$

$$\frac{1}{2M_0} J_k^{(disc)} = J_k^{(2)}, \quad (34)$$

and at zero momentum on the lattice,

$$\langle J_k^{(3)} \rangle = \langle J_k^{(4)} \rangle. \quad (35)$$

Thus, the 6 vector matrix elements can be reconstructed from the subset  $j = 0, 1, 3$ . For the purpose of analysing the individual contributions to the vector decay constant of the matrix elements 24- 28 and 31, we define,

$$f_V^{(j)} \sqrt{M_V} = \frac{1}{\sqrt{M_V}} \langle 0 | J_k^{(j)} | V_k \rangle. \quad (36)$$

We use  $f_V \sqrt{M_V}$  to denote the total decay constant at both tree-level and 1-loop.

The matching coefficients  $C_j$  and  $C_A$ , and  $C_{Vj}$  and  $C_V$ , have been evaluated to 1-loop in perturbation theory by Morningstar and Shigemitsu [15,16]. These coefficients depend on  $M$  and  $\alpha$ , where we take  $\alpha_V(q^*)$  [28] for the strong coupling. The scale  $q^*$  also depends on the heavy quark mass. This scale is unknown at present, although in the static limit Hernandez and Hill found that,  $q^* = 2.18/a$  [29]. At this stage, we assume that  $q^*$  for each mass lies somewhere between  $1/a$  and  $\pi/a$ , and compute  $f_{PS}$  and  $f_V$  for these two limits.

The coefficients  $C_0$  and  $C_1$  in the pseudoscalar case, and  $C_{V0}$ ,  $C_{V1}$ ,  $C_{V2}$  and  $C_{V4}$  in the vector case, include a term  $\alpha \ln(aM)/\pi$ . When computing  $f_B$  and  $f_{B^*}$  we insert  $aM_0$  for the heavy quark mass. There are no problems with large logarithms for the quark masses used in this study, however, for larger  $M$ , resumming the logarithms would be more appropriate. A different approach is needed when extracting the slope of the decay constants and comparing with the static limit. In this case, it is assumed that the meson simulated at each  $M_0$  is the  $B$  meson (to a better or worse approximation), and thus,  $aM_0^b$  must be inserted in the logarithms for all heavy quark masses.

A possible concern is that the  $\alpha/(aM)^n$  terms in the coefficients combine with nonperturbative lattice errors,  $\propto (a\Lambda_{QCD})^n$  in the matrix elements  $\langle J_L^{(0)} \rangle$  or  $\langle J_k^{(0)} \rangle$ . This, then, leads to contributions that look like physical  $(\Lambda_{QCD}/M)^n$  corrections to  $f_B$  or  $f_{B^*}$ . However, since  $\langle J_L^{(0)} \rangle$  and  $\langle J_k^{(0)} \rangle$  are designed to match full QCD through  $O(\alpha a)$ , these errors appear at  $O(\alpha^2(a\Lambda_{QCD}))$  or  $O((a\Lambda_{QCD})^2)$ . The leading contribution to  $f_B$  or  $f_{B^*}$  from these errors is beyond the order in the NRQCD series considered here. These issues have been discussed previously, in more detail, in references [3] and [15].

Theoretically, within HQET, the decay constants in the combinations,  $f_{PS}\sqrt{M_{PS}}$  and  $f_V\sqrt{M_V}$ , are non-zero and equal in the static limit, reflecting spin and flavour symmetry. Away from this limit,  $O(1/M)$  corrections take the form:

$$f\sqrt{M} = (\alpha(M))^{-1/(2\beta_0)}(f\sqrt{M})^\infty (1 + C/M + \dots) \quad (37)$$

where the decay constant in the static limit,  $(f\sqrt{M})^\infty$ , and the coefficient of the linear slope,  $C$ , are expected to be of  $O(\Lambda_{QCD})$ . Thus, the ratio of the vector to pseudoscalar decay constant can be expressed as:

$$f_V\sqrt{M_V}/f_{PS}\sqrt{M_{PS}} = 1 + (C_V - C_{PS})/M + \dots \quad (38)$$

Another quantity to consider is the ratio of the pseudoscalar decay constants for the heavy-light mesons containing a  $u$  light quark and that containing a  $s$  quark,

$$\frac{f_{PS}\sqrt{M_{PS}}|_{\kappa_s}}{f_{PS}\sqrt{M_{PS}}|_{\kappa_c}} = \left( \frac{f_{PS}\sqrt{M_{PS}}|_{\kappa_s}}{f_{PS}\sqrt{M_{PS}}|_{\kappa_c}} \right)^\infty (1 + (C_{PS}^{\kappa_s} - C_{PS}^{\kappa_c})/M + \dots). \quad (39)$$

Since the heavy quark is almost a spectator in the heavy-light meson, the shift in the decay constant when the light quark mass is changed is expected to be roughly independent of  $M$ . Thus,  $C_{PS}|_{\kappa_s}$  is approximately equal to  $C_{PS}|_{\kappa_c}$ , and the ratio should have little dependence on the heavy quark mass.

The contributions to the slope of the decay constants from the  $O(1/M)$  terms in the NRQCD action and corrections to the current can be identified. From first order perturbation theory in  $1/M$  about the static limit:

$$C = G_{kin} + 2d_M G_{hyp} + d_M G_{corr}/6, \quad (40)$$

where  $d_M = 3$  and  $-1$  for pseudoscalar and vector mesons respectively. Thus,

$$C_{PS} - C_V = 8G_{hyp} + 2G_{corr}/3. \quad (41)$$

The kinetic and hyperfine terms contribute to the decay constant through the correction to the meson wavefunction.

$$\begin{aligned} \langle 0 | q^\dagger \Gamma^{(2)} \psi | P \rangle_\infty G_{kin} = \\ \langle 0 | \int dy T \{ q^\dagger \Gamma^{(2)} \psi(0), \mathcal{O}_{kin}(y) \} | P \rangle_\infty, \end{aligned} \quad (42)$$

$$\begin{aligned} \langle 0 | q^\dagger \Gamma^{(2)} \psi | P \rangle_\infty 2d_M G_{hyp} = \\ \langle 0 | \int dy T \{ q^\dagger \Gamma^{(2)} \psi(0), \mathcal{O}_{hyp}(y) \} | P \rangle_\infty, \end{aligned} \quad (43)$$

while  $G_{corr}$  is directly related to the tree-level current correction:

$$\langle 0 | q^\dagger \Gamma^{(2)} \psi | P \rangle_\infty d_M G_{corr} / 6 = \langle 0 | q^\dagger \Gamma^{(2)} \frac{\sigma \cdot \vec{D}}{2} \psi | P \rangle_\infty. \quad (44)$$

$|P\rangle_\infty$  represents the meson in the limit of infinite heavy quark mass and  $\Gamma^{(2)} = 1$  and  $\sigma$  for the pseudoscalar and the vector, respectively. Note that equations 42-44 are tree level expressions. This analysis is discussed in more detail in reference [9].

## A. Results

The bare lattice matrix elements computed in the lattice simulation,  $f_{PS}^{(0,1)} \sqrt{M_{PS}}$  and  $f_V^{(0,1,3)} \sqrt{M_V}$ , are given in the appendix in tables VI and VII for the pseudoscalar, and tables VIII, IX and X for the vector, for the range of masses studied. Combined with the appropriate matching factors, we obtain the tree-level and renormalised decay constants shown in tables XI and XII, for the pseudoscalar and vector respectively.

Considering, initially,  $aM_0 = 2.0$ , a quark mass in the region of the  $b$  quark mass ( $aM_0^b = 2.1$  for  $a^{-1} = 2.0$  GeV), table XI shows that  $f_{PS} \sqrt{M_{PS}}$  is reduced from the tree-level value by 10% for  $aq^* = \pi$  and 16% for  $aq^* = 1.0$ . Thus, the combined 1-loop corrections to the decay constant,  $O(\alpha)$ ,  $O(\alpha a)$  and  $O(\alpha/M)$ , are significant but not larger than expected. In addition, the uncertainty in  $f_B$  due to the unknown  $q^*$  is not unduly large,  $\sim 6\%$ , although it is bigger than the statistical errors of  $\sim 3\%$ .

We study the tree-level and renormalised currents further by analysing the individual contributions to the  $PS$  decay amplitude from the various operators and matching factors. Table XIII, details the percentage correction of these contributions to the zeroth order tree-level matrix element,  $\langle J_L^{(0)} \rangle$ ;  $aM_0 = 2.0$  and  $aq^* = 1.0$  is used for the 1-loop terms. Note that the contributions from  $J_L^{(2)}$  and  $J_L^{disc}$  are reconstructed from  $\langle J_L^{(1)} \rangle$ .

From the table we see that the  $O(1/M)$  tree-level correction,  $\langle J^{(1)} \rangle$ , reduces the decay constant by 13%. The 1-loop correction for this matrix element is small,  $\sim 1\%$ , however, the other 1-loop terms, the  $O(\alpha)$  correction to  $\langle J^{(0)} \rangle$ ,  $\alpha \rho_0$ , and the  $O(\alpha/M)$  matrix element and the  $O(\alpha a)$  discretisation correction,  $\alpha \rho_2 \langle J^{(2)} \rangle + \alpha \langle J^{disc} \rangle$ , are all of a similar magnitude to the tree-level correction, around 10%. However, none of the terms are unduly large and there is no indication that NRQCD is breaking down. Since the terms contribute with different signs there is some cancellation between them and the combined 1-loop correction is  $-14\%$  for  $aq^* = 1.0$ , the same size as the  $O(1/M)$  tree-level correction. Thus, the total correction to  $f_{PS}^{(0)} \sqrt{M_{PS}}$  is  $-27\%$ ; this falls to  $-21\%$  for  $aq^* = \pi$ , of which  $-8\%$  is due to the 1-loop terms.

The picture is fairly similar for the vector decay constant. Table XII shows  $f_V \sqrt{M_V}$  at  $aM_0 = 2.0$  is reduced from the tree-level value by 14% and 22% when the matching factors are included with  $aq^* = \pi$  and 1.0, respectively; the dependence on  $q^*$  is moderate. In the

tree-level case,  $f_{PS}\sqrt{M_{PS}}$  is slightly below  $f_V\sqrt{M_V}$ , while for the same  $q^*$  they are roughly equal. However, there is no reason for the characteristic scale for the vector to be the same as that for the pseudoscalar, and thus, it is difficult to compare the two at this stage.

The contributions to the vector decay constant from the individual matrix elements and matching coefficients are also detailed in table XIII. We see that the 1-loop terms,  $\alpha\rho_0$  and  $\alpha\rho_2\langle J^{(2)}\rangle + \alpha\langle J^{disc}\rangle$  are all the same order of magnitude as in the  $PS$  case, and combine to give a  $-20\%$  correction to the zeroth order vector current. The remaining 1-loop terms, all  $O(\alpha/M)$ , are very small, of order 1%. However, since the  $O(1/M)$  tree-level term is smaller and with opposite sign, compared to the  $PS$  case, the overall correction to  $\langle J^{(0)}\rangle$  is smaller:  $-17\%$  ( $-10\%$ ) for  $aq^* = 1.0$  ( $\pi$ ). The relative size of the individual corrections compared to those for the  $PS$  is discussed later.

Interpolating the results for  $f_{PS}\sqrt{M_{PS}}$  and  $f_V\sqrt{M_V}$  to  $M_0 = M_0^b$ , and converting into physical units we obtain the values for  $f_B$  and  $f_{B^*}$  shown in table XIV; the results for  $f_{B_s}$  and  $f_{B_s}/f_B$  are also given. Table XIV presents the predictions for the decay constants derived using both  $a^{-1} = 2.0$  and  $2.4$  GeV. We take the difference in the decay constants for the different choices of lattice spacing as an estimate of the error in  $f_B$  due to uncertainty in the scale.

Combined with estimates of the other dominant systematic errors, detailed in table I, our predictions for the pseudoscalar and vector decay constants are:

$$f_B = 186(5)(19)(9)(13)(+50) \text{ MeV} \quad (45)$$

$$f_{B_s} = 215(3)(22)(9)(15)(+49)(-5) \text{ MeV} \quad (46)$$

$$f_{B^*} = 181(6)(18)(9)(13)(+55) \text{ MeV} \quad (47)$$

$$f_{B_s^*} = 213(4)(21)(9)(15)(+60)(-4) \text{ MeV} \quad (48)$$

The first error is statistical. The second is the estimate of the  $O(\alpha^2)$  perturbative error  $\sim 10\%$ . The third and fifth errors are the estimates of uncertainty arising from the light quark discretisation errors and the uncertainty in  $a^{-1}$ . Note that the latter includes the corresponding change in  $aM_0^b$ . For  $f_{B_s}$  there is an additional error due to the uncertainty in  $\kappa_s$ .

The fourth error is due to the truncation of the NRQCD series. To estimate this, one must consider the next order corrections,  $O(1/M^2)$ , to the current and to the NRQCD action (given in equation 4). Naively, one expects these terms to be of order  $\sim 1\%$ . As mentioned in section III Ishikawa et al [12] performed a tree-level analysis of the  $O(1/M^2)$  terms for  $f_{PS}$  and  $f_V$ . These authors found that in the region of the  $B$  meson  $\delta H_{h.o.}$  had no effect on the  $PS$  or  $V$  matrix elements. For lighter values of  $aM_0$  the higher order terms in the action tended to increase the matrix elements.

The individual tree-level current corrections are,

$$J^{(a)} = \frac{1}{8M_0^2}\bar{q}\Gamma D^2Q, \quad (49)$$

$$J^{(b)} = \frac{1}{8M_0^2}\bar{q}\Gamma g\vec{\Sigma} \cdot \vec{B}Q, \quad (50)$$

$$J^{(c)} = -\frac{1}{8M_0^2}\bar{q}\Gamma 2ig\vec{\alpha} \cdot \vec{E}Q, \quad (51)$$



where  $\vec{\alpha} = \gamma_0 \vec{\gamma}$  and  $\vec{\Sigma} = \text{diag}(\vec{\sigma}, \vec{\sigma})$ .  $\Gamma = \gamma_5 \gamma_0$  and  $\gamma_k$  for the pseudoscalar and vector respectively. These terms were each found to be less than 2% in magnitude. The corrections contribute with differing signs and there is a cancellation between them which leads to a small overall decrease in  $f_B \sqrt{M_B}$  of  $\sim 3\%$ . Since at  $O(1/M)$  the 1-loop terms are as large as those at tree-level, as discussed previously, we estimate the overall uncertainty in the decay constants due to the omitted  $O(1/M^2)$  and  $O(\alpha/M^2)$  terms as 6%.

In total, adding the statistical and systematic errors in quadrature, there is a 14% uncertainty in the decay constants. This is much smaller than the  $\sim 30\%$  error due to the uncertainty in  $a^{-1}$ . Thus, a determination of  $f_B$  of around  $\sim 10\%$  is possible, but only if the systematic error in  $a^{-1}$  is reduced significantly.

In contrast,  $f_{B_s}/f_B$  and  $f_{B_s^*}/f_{B^*}$  are quantities for which most systematic errors cancel out. These ratios are independent of the heavy quark mass (see below), while table XIV indicates that it is insensitive to the 1-loop corrections. Furthermore,  $f_{B_s}/f_B$  and  $f_{B_s^*}/f_{B^*}$  are not dependent on the lattice spacing. The only significant error is that due to the uncertainty in  $\kappa_s$ . We find,

$$f_{B_s}/f_B = 1.14(2)(-2), \quad (52)$$

$$f_{B_s^*}/f_{B^*} = 1.14(2)(-2) \quad (53)$$

where the first error is statistical and the second is due to  $\kappa_s$ .

We now study the dependence of  $f_{PS} \sqrt{M_{PS}}$  on the light and heavy quark mass. Considering the light quark mass dependence initially, we find the decay constant is linearly dependent on  $m_q$  as shown in an example of the chiral extrapolation of this quantity in the appendix for  $aM_0 = 1.0$ . As discussed in section V the dependence on  $am_q$  is expected to be roughly the same for all  $aM_0$ , i.e.  $C_{PS}$  is insensitive to the light quark mass. Figure 5 gives the tree-level values for  $f_{PS} \sqrt{M_{PS}}$  for all heavy quark masses and  $\kappa_l$ .

We perform a fit to the decay constant for fixed  $\kappa_l$  using a functional form motivated by equation 37,

$$f_{PS} \sqrt{M_{PS}} = C_0 + C_1/M + \dots \quad (54)$$

where  $C_0 = (f\sqrt{M})^\infty$  and  $C_1/C_0 = C_{PS}|_{\kappa_l}$ . The slopes for each  $\kappa_l$  and the chiral limit are given in table XV. We find the slope for the lighter two  $\kappa$ 's (corresponding to  $m_q \sim m_s$  and smaller) are consistent with the chiral limit,  $C_{PS} \sim 1$  in lattice units. However, from the results for  $\kappa_l = 0.1385$ , we see there is a much stronger dependence of the decay constant on  $1/(aM_{PS})$  for  $m_q$  heavier than  $m_s$ , although with such large errors it is only a  $2\sigma$  effect. This behaviour may be due to discretisation errors in  $C_{PS}$  (which is a light quark quantity) arising from the light quark action, which increase with the mass of the light quark:  $O(\alpha am_q)$  and  $O((am_q)^2)$  for the clover action. Since  $C_{PS}|_{\kappa_s} \approx C_{PS}|_{\kappa_c}$ , the ratio  $(f_{PS} \sqrt{M_{PS}})_{\kappa_s} / (f_{PS} \sqrt{M_{PS}})_{\kappa_c}$ , has almost no dependence on the heavy quark mass, as seen in figure 5 (b).

The heavy quark mass dependence of  $f_{PS} \sqrt{M_{PS}}$  at tree-level and 1-loop is compared in figure 6 for  $\kappa_l = \kappa_c$ . In the tree-level case there is a steep dependence on the heavy quark mass, and this, initially suggested higher orders in the heavy quark expansion would be needed at the  $B$  meson [9];  $f_{PS} \sqrt{M_{PS}}$  is reduced from the static limit by  $\sim 35\%$  at

the  $B$  meson. However, figure 6 shows the slope is dramatically reduced when the 1-loop corrections are included;  $f_{PS}\sqrt{M_{PS}}$  at the  $B$  meson is reduced by  $\sim 17\%$  compared to the static limit for  $aq^* = \pi$ , while there is almost no dependence on  $M$  for  $aq^* = 1.0$ .

We perform a fit to the data sets using equation 54, the results are detailed in table XVI. The relative slope at tree-level is  $\sim -1$  in lattice units or  $\sim -2$  GeV, using  $a^{-1} = 2.0$  GeV. This is well above the naive expectation of  $-300$  to  $-500$  MeV ( $O(\Lambda_{QCD})$ ). However, at 1-loop this is reduced to anywhere between  $-1$  GeV and 0, depending on  $q^*$ . Note that  $q^*$  depends on the mass, and this dependence must be determined before the slope can be extracted correctly. However, the results with fixed  $q^*$  provide a rough bound on the size of the slope. Previous calculations in the quenched approximation using the clover action and the Fermilab approach [6] find the slope to be close to the upper limit around  $-1$  GeV [30–33]. Note that the values of  $q^*$  are also not known for this method.

There are clear advantages to simulating at finite heavy quark mass with an inverse lattice spacing around 2.0 GeV. The combined 1-loop corrections grow as  $M$  tends towards the static limit (with the  $\alpha \ln(aM)/\pi$  terms in the matching coefficients fixed to  $\alpha \ln(aM_0^b)$ ), as does the accompanying uncertainty due to the omission of higher orders in the matching coefficients. Thus, for a coarser lattice spacing, i.e. with a larger value for  $aM_0^b$ , (and indeed for the static limit) a nonperturbative determination of the matching factors becomes essential. Certainly this is required for a determination of the slope of the decay constant. For a finer lattice,  $aM_0^b$  becomes smaller, and at some point NRQCD breaks down: the bare lattice matrix elements grow larger, i.e. increasingly higher orders in the NRQCD expansion become important, while the  $\alpha/(aM)$  terms in the matching coefficients also become large and perturbation theory is not well controlled.

The interplay between the individual  $PS$  matrix elements and their effect on the slope of the decay constant can be seen in figure 7. The tree-level and 1-loop corrections to the zeroth order matrix element are shown (as percentages) as a function of  $1/(aM_0)$  for  $aq^* = 1.0$ . The  $O(1/M)$  and  $O(\alpha/M)$  terms,  $\langle J^{(1)} \rangle$  and  $\alpha\rho_2 \langle J^{(2)} \rangle$  and  $\alpha\rho_1 \langle J^{(1)} \rangle$ , respectively, vanish in the static limit and grow as  $aM_0$  becomes small. The discretisation correction has very little dependence on the heavy quark mass, while the  $O(\alpha)$  correction to  $\langle J^{(0)} \rangle$  decreases dramatically from the static limit, and goes through zero as  $aM_0$  becomes lighter.

The corrections contribute with differing signs leading to some cancellation between them. Towards the heavy mass limit,  $1/(aM_0) < 0.5$ , the  $O(1/M)$  and  $O(\alpha/M)$  terms approximately cancel each other. This leaves the  $O(\alpha)$  and  $O(a\alpha)$  terms which are both large in this region,  $\sim -20\%$  each, leading to a very large 1-loop correction to  $f_{PS}^{(0)}\sqrt{M_{PS}}$ . In contrast, for the lighter values of  $aM_0 < 1.2$ ,  $\alpha\rho_0$  is much smaller, while the  $O(\alpha/M)$  terms are now large enough to approximately cancel the discretisation correction. Thus, surprisingly, at  $1/aM_{PS} \sim 0.6$ , the decay constant is roughly equal to the tree-level value. Note, however, that in this region the 1-loop terms  $\alpha\rho_2 \langle J^{(2)} \rangle$  and  $\langle J^{disc} \rangle$  are not small at around 10%.

Thus, the almost complete removal of any heavy quark mass dependence when the 1-loop terms are included using  $aq^* = 1.0$ , is due to the large 1-loop correction in the large mass limit (where  $O(1/M)$  terms are small),  $\sim -40\%$  in the static limit, and a large tree-level  $O(1/M)$  correction for the lighter meson masses (where the 1-loop terms cancel),  $\sim -30\%$  for  $aM_0 = 0.8$ . Since the tree-level correction is so large for the lighter meson masses, higher

orders in the NRQCD expansion should be considered in this region.

The vector decay constant behaves in a similar way as a function of the heavy quark mass to the pseudoscalar. Figure 8 details the individual percentage corrections to  $f_V^{(0)}\sqrt{M_V}$  versus  $1/(aM_0)$ . The bare matrix elements,  $\langle J_k^{(i)} \rangle$ ,  $i = 1, 4$  are related to each other as given in equations 33- 35. In the heavy quark limit, these expressions simplify and furthermore one finds additional relations between the vector and pseudoscalar current corrections. If we re-write  $J_k^{(1)}$  and  $J_k^{(3)}$  in the form,

$$J_k^{(1)} = -\frac{1}{2M_0}\bar{q}(-\gamma_\perp \cdot D_\perp + \gamma_k D_k)\gamma_k Q \quad (55)$$

$$J_k^{(3)} = -\frac{1}{2M_0}\bar{q}\gamma_k D_k\gamma_k Q \quad (56)$$

and take  $|V_k\rangle = [Q^\dagger\gamma_k q]|0\rangle$ , then by assuming that the contraction of  $QQ^\dagger$  is spin diagonal (in the large M limit) we can deduce,

$$\langle 0|\bar{q}(\gamma_i D_i)\gamma_k Q|V_k\rangle \quad (i \neq k) = \langle 0|\bar{q}(\gamma_k D_k)\gamma_k Q|V_k\rangle, \quad (57)$$

i.e.  $\langle J_k^{(1)} \rangle = -\langle J_k^{(3)} \rangle$ . Tables IX and X show that our results agree with this relation for the heavier values of  $M \gtrsim 3.0$ . Thus, equation 33 reduces to  $\langle J_k^{(2)} \rangle = 3\langle J_k^{(3)} \rangle = -3\langle J_k^{(1)} \rangle$ .

Following the same argument, and taking  $|PS\rangle = [Q^\dagger\gamma_5 q]|0\rangle$ , one can show that  $\langle J_L^{(2)} \rangle$  for the PS is equal to  $\langle J_k^{(2)} \rangle$  for the V,

$$\langle 0|\bar{q}(\gamma_j \overleftarrow{D}_j)\gamma_0\gamma_k Q|V_k\rangle = \langle 0|\bar{q}(\gamma_j \overleftarrow{D}_j)\gamma_5\gamma_0 Q|PS\rangle \quad (58)$$

for any  $j$ . Thus the corresponding discretisation corrections are also equal,  $\langle J_k^{(disc)} \rangle = \langle J_L^{(disc)} \rangle$ , and  $\langle J_L^{(1)} \rangle = \langle J_L^{(2)} \rangle = -3\langle J_k^{(1)} \rangle$ ; the latter clearly comes from spin-symmetry. The results in figures 7 and 8 in the large mass limit agree with these expressions. In general the terms which spoil equations 57 and 58 at finite  $M$  are due to the  $O(1/M)$  terms in the action modifying the meson wavefunction from the static limit (as in equation 43 and 42 for the PS decay constant), and are small since they appear as an  $O(1/M)$  correction to the matrix element.

## B. Making contact with HQET

As discussed in section V, one can attempt to analyse the  $1/M$  corrections to the static limit within the framework of HQET. Equations 40 and 41 suggest that by taking appropriate combinations of  $f_{PS}\sqrt{M_{PS}}$  and  $f_V\sqrt{M_V}$ ,  $G_{kin}$  and  $G_{hyp}$  can be separated; since  $\langle J^{(1)} \rangle$  is calculated separately  $G_{corr}$  can easily be obtained. In particular, the spin average of the  $PS$  and  $V$  decay constants (without  $\langle J^{(1)} \rangle$ ),  $f\sqrt{M}$ , cancels the hyperfine contribution, and the slope of this quantity is purely determined by  $G_{kin}$ . Conversely, the ratio of these quantities cancels  $G_{kin}$  and a determination of the slope gives  $G_{hyp}$ .

Note that the renormalisation factors calculated by Morningstar and Shigemitsu are not those required for a detailed investigation of spin and flavour symmetry within HQET. In

references [15] and [16] the lattice NRQCD matrix elements are matched directly to full QCD while, the factors matching lattice NRQCD to continuum HQET are the ones that are needed. In particular, only the tree-level decay constants will obey the spin symmetry relation that the ratio of  $V$  to  $PS$  is 1 in the static limit. Thus, we restrict ourselves to a tree-level analysis of spin symmetry and the origin of the slope  $C$ . One-loop matching to full QCD would introduce a short distance correction factor to the ratio  $f_V\sqrt{M_V}/f_{PS}\sqrt{M_{PS}}$  of  $\eta_{static} = [1 - \alpha(8/(3\pi))]$ .

Figure 9 presents the results for  $f\sqrt{M}$ , compared to the  $PS$  decay constant, with and without the tree-level  $O(1/M)$  current correction. In the heavy mass limit, all three quantities converge indicating the dominant contribution to the tree-level  $C_{PS}$  is from  $G_{kin}$ . The figure also shows  $f_{PS}\sqrt{M_{PS}}/f_V\sqrt{M_V}$ . Without  $\langle J^{(1)} \rangle$  this ratio is positive (indicating  $G_{hyp}$  is positive) and tends to 1 in the static limit, consistent with spin-symmetry; when the current correction is included  $f_V\sqrt{M_V} < f_{PS}\sqrt{M_{PS}}$ .  $G_{corr}$  can be very accurately determined by extrapolating  $2M_0 \langle J^{(1)} \rangle$  to the static limit, displayed in figure 9 (c).

We perform fits to these combinations of  $PS$  and  $V$  decay constants and extract  $G_{kin}$ ,  $G_{hyp}$  and  $G_{corr}$ . The results are given in table XVII. Note that only the slopes of physical combinations of the decay constants, i.e.  $f_{PS}\sqrt{M_{PS}}$ ,  $f\sqrt{M}$  and  $f_{PS}\sqrt{M_{PS}}/f_V\sqrt{M_V}$ , are expected to be  $O(a\Lambda_{QCD})$ . The ratio of decay constants is roughly in agreement with this picture; the slope of the ratio is small, while  $G_{corr}$  and  $G_{hyp}$  are individually much larger. However, the physical decay constants themselves, dominated by  $G_{kin}$ , have a much larger slope. Considering the strong dependence on  $M$  of the  $O(\alpha)$  correction to  $f_{PS}^{(0)}\sqrt{M_{PS}}$  seen in the results of Morningstar and Shigemitsu,  $G_{kin}$  is likely to be significantly affected by renormalisation. Similarly, the 1-loop corrections to  $G_{corr}$  are likely to be large.

The results in table XVII through the use of the clover action for the light quarks and extrapolating to the chiral limit, are an improvement on our previous results with Wilson light fermions published in reference [9]. Numerically, the difference between the results is mainly due to the extrapolation to  $\kappa_c$  in the clover case <sup>2</sup>, since at tree-level the decay constant does not change significantly between the two light quark actions.

### C. $n_f$ dependence

We compare our results with those calculated as part of the  $O(1/M^2)$  quenched simulation at  $\beta^{n_f=0} = 6.0$  already mentioned in section IV A. In reference [3] we quote,

$$f_B = 147(11)({}_{-12}^{+8})(9)(6) \text{ MeV} \quad (59)$$

$$f_{B_s} = 175(08)({}_{-10}^{+7})(11)(7)({}_{-0}^{+7}) \text{ MeV} \quad (60)$$

$$f_{B_s}/f_B = 1.20(4)({}_{-0}^{+4}) \quad (61)$$

for the quenched result. The errors are calculated in a similar way to those in this paper and, with the exception of the uncertainty due to fixing  $a^{-1}$ , are of a similar size. The first error

---

<sup>2</sup>The Wilson results in reference [9] correspond to a light quark mass greater than  $m_s$  and thus the slope of the decay constant is much larger than in the chiral limit, as discussed previously.

corresponds to statistical errors and those errors due to extrapolation/interpolation in  $\kappa$  and  $aM_0$ . The second error indicates the uncertainty in  $a^{-1}$  calculated using  $a^{-1} = 2.0$  GeV and 1.8 GeV. This range represents the spread in  $a^{-1}$  derived from various light spectroscopic quantities. Higher order perturbative and relativistic uncertainties are given by the third error and the fourth error is due to discretisation corrections. For  $f_{B_s}$  the error in fixing  $\kappa_s$  is found by fixing the strange quark mass from the  $K$  meson (for the central value) and the  $\phi$  meson; the  $K^*$  meson gave the same value of  $\kappa_s$  as the  $\phi$  meson.

The quenched calculation includes  $\delta H_{h.o.}$  in the action and the tree-level  $O(1/M^2)$  current corrections. Since the  $O(1/M^2)$  current corrections were calculated separately we can easily omit them in order to make a better comparison with our present  $O(1/M)$   $n_f = 2$  results. Apart from this the quenched simulation and analysis remains the same as detailed in reference [3]. The modified quenched results are presented in table XVIII. As mentioned in section V A, the contributions from  $\delta H_{h.o.}$  have a minimal effect on the pseudoscalar matrix elements in the region of the  $B$  meson. Thus, there should only be a very small uncertainty in the comparison between quenched and  $n_f = 2$  results due to the differing actions. In fact, since  $\delta H_{h.o.}$  tends to increase  $f_B$ , removing it would increase rather than decrease the sea quark effect that we see.

The comparison is made at tree-level, and at 1-loop for  $aq^* = \pi$  and  $aq^* = 1.0$  in table XVIII. In perturbation theory the effects of sea quarks appear beyond 1-loop. Thus,  $aq^*$  is likely to be very similar for the same  $Ma$  values for quenched and  $n_f = 2$ . Since the values of  $a$  and hence  $aM_0^b$  are closely matched for the two simulations, it is reasonable to compare at fixed  $aq^*$ .

Considering, in addition, that the quenched and unquenched simulations are very similar in method and analysis we expect the systematic errors to be similar (and correlated) in both cases. Thus, initially, we make a comparison considering only the statistical errors. Table XVIII shows that  $f_B$  is a quantity which is sensitive to the presence of sea quarks and that the quenched value for  $f_B$  may be substantially lower than the value in full QCD. We find a 23–25% or  $> 3\sigma$ <sup>3</sup> increase in  $f_B$ , when two flavours of sea quarks are included. The increase is roughly the same at tree-level and at 1-loop for  $aq^* = \pi$  and  $aq^* = 1.0$ . If the actual value of  $aq^*$  for  $n_f = 0$  turns out to be higher than that for  $n_f = 2$  then the sea quark effect becomes smaller. In the reverse case the effect would be larger.

Alternatively, we can ignore the fact that the systematic errors between the quenched and unquenched results are probably highly correlated. Combining the statistical and systematic errors in quadrature, we obtain  $f_B = 149(19)$  MeV at  $n_f = 0$ , compared to 186(25) MeV at  $n_f = 2$ ; the lattice spacing is fixed using  $m_\rho$  in both cases, i.e. the uncertainty arising from fixing  $a$  is ignored, and the central value is obtained from the average of the results for  $aq^* = 1.0$  and  $\pi$ . In this case, the 27 MeV shift in  $f_B$  is a  $1\sigma$  effect. Note that, considering the uncertainty in  $a^{-1}$  for  $n_f = 2$ , using  $a^{-1} = 2.4$  GeV will lead to a larger sea quark effect. This increase includes any effect due to finite volume problems for the determination of  $a^{-1}$  from  $m_\rho$  at  $n_f = 2$ . As mentioned in section III  $a^{-1}$  is expected to be underestimated if the

---

<sup>3</sup>The significance of the shift in the decay constant is found by comparing the difference between  $f_B$  at  $n_f = 2$  and 0 with the statistical errors added in quadrature.

$\rho$  meson is squeezed.

Comparing the central values for  $f_{B_s}$  the increase with  $n_f$  is slightly smaller,  $\sim 20\%$ , but statistically more significant at between 5 and  $6.5\sigma$ . The error in  $f_{B_s}$  due to the uncertainty in  $\kappa_s$  clouds the comparison for this quantity slightly. For the  $n_f = 2$  configurations,  $m_\phi$  and  $m_K$  give consistent values for  $\kappa_s$ , while  $m_{K^*}$  gives a slightly higher value (see section II). In contrast, for the quenched results the error in  $\kappa_s$  is larger, and as mentioned previously, is computed using from using  $m_K$  and  $m_\phi$ ;  $m_{K^*}$  and  $m_\phi$  give consistent results. Thus, if  $m_\phi$  is used the quenched decay constant is increased by 7 MeV, while the  $n_f = 2$  value is unchanged. The difference between the two values for  $f_{B_s}$  is reduced to 14–16% or a 4–5.5 $\sigma$  effect (a similar decrease is found using  $m_{K^*}$ ). A detailed study of how to fix  $\kappa_s$  is needed to improve the comparison of quenched and unquenched results for  $f_{B_s}$ . If the systematic errors are taken in account,  $f_{B_s} = 180(20)$  MeV at  $n_f = 0$  and 215(29) MeV for  $n_f = 2$ ; the central value is found using  $\kappa_s$  from  $m_K$ , but the associated uncertainty in  $\kappa_s$  is included in the error. Assuming the errors are independent, the 35 MeV shift corresponds to  $1\sigma$ .

The effect of sea quarks in the decay constants have also been studied by the MILC collaboration [34].  $f_B$  was found to increase by  $\sim 13\%$  from the quenched to the  $n_f = 2$  result. The Wilson action was employed for the heavy and light quark at several  $\beta$  values at both  $n_f = 0$  and 2. Extrapolating the results to the continuum limit these authors find  $f_B = 159(11)(stat)(+22 - 9)(sys)(+21 - 0)(quench)$  MeV. Clearly systematic errors (of which discretisation errors are the dominant source) are as large an effect as quenching. In this situation the size of the sea quark effects is very sensitive to the interpolation of the  $n_f = 0$  results to a lattice spacing which coincides with that found at  $n_f = 2$  to enable a comparison. However, until the systematic errors are explored thoroughly at  $n_f = 2$ , the difference between our results and those from the MILC collaboration are not significant.

Since the matching factors have been calculated over a wide range of  $M$ , we can also investigate the mass dependence of the sea quark effects. Figure 10 presents the results for tree-level and 1-loop for two values of  $aq^*$ . The roughly constant shift between  $n_f = 0$  and  $n_f = 2$  for the whole range of meson masses from  $\sim M_B/3$  to  $4M_B$  indicates the sea quark effects are associated with the light quark rather than dependent on the heavy quark. We also compare the results for the ratio  $f_{B_s}/f_B$ . The large sea quark effects we see in  $f_{B_s}$  and  $f_B$  individually appear to cancel in the ratio. There is only a  $\sim 5\%$  or  $1.3\sigma$  decrease in  $f_{B_s}/f_B$  when two flavours of sea quarks are introduced. If  $\kappa_s$  from  $m_\phi$  is used the results are consistent to within less than  $0.5\sigma$ .

## VI. CONCLUSIONS

We presented comprehensive results for the spectrum and decay constants of the  $B$  meson including the effects of two flavours of dynamical quarks. In addition, an investigation of the effects of sea quarks through a comparison with quenched simulations was performed. At present, we do not attempt to extrapolate in  $n_f$  but look for initial indications of quenching effects.

Results, summarised in table III, were presented for the lower lying  $S$  and  $P$  meson states and the  $\Lambda_b$  baryon. With the exception of the  $\Lambda_b$ – $B$  splitting, the estimates of the systematic errors for all mass splittings were comparable to or less than the statistical

errors. The  $\Lambda_b-B$  splitting represented the only significant disagreement with experiment. This discrepancy is probably due to finite volume effects.

A detailed analysis of the heavy quark mass dependence of physical spectral mass splittings was performed. We found the behaviour with  $M$  to fulfill the naive expectation:  $O(\Lambda_{QCD})$  quantities are weakly dependent on  $M$ , while spin-dependent splittings vanish as  $1/M$  in the large mass limit. Estimates of the slope and intercept of these quantities were extracted and agreement was found with the theoretical expectation from HQS. A comparison was also made with experiment. This showed that the slope for the hyperfine splitting was too low in our simulation. Residual quenching effects are a possible explanation for this discrepancy. However, we have underestimated the splitting through the use of the tree-level value of the coefficient of the hyperfine term in our simulation (this underestimate is not significant within statistics at the  $B$  meson).  $c_B$  depends on  $M$  and improved estimates of this coefficient must be included for all  $aM_0$  before the origin of the discrepancy is clear.

We presented a comparison of our results with a similar quenched calculation at  $\beta^{n_f=0} = 6.0$  using a  $O(1/M^2)$  action detailed in [2]. A comparison with a higher order NRQCD action is possible as the additional terms in the action do not significantly affect the mass splittings considered. The quenched results reproduce the experimental spectrum well to the present level of accuracy, and there is no significant difference between the quenched and  $n_f = 2$  results.

In addition, results were presented for the  $f_B$ ,  $f_{B_s}$ ,  $f_{B^*}$  and  $f_{B_s^*}$  decay constants at tree-level and fully consistent to 1-loop in perturbation theory. We found the combined 1-loop corrections are moderate and reduce the tree-level value of  $f_B$  by 10–16% depending on  $q^*$ . Our predictions for the  $PS$  and  $V$  decay constants are

$$\begin{aligned} f_B &= 186(5)(stat)(19)(pert)(9)(disc)(13)(NRQCD)(+50)(a^{-1}) \text{ MeV}, \\ f_{B_s} &= 215(3)(stat)(22)(pert)(9)(disc)(15)(NRQCD)(+49)(a^{-1})(-5)(\kappa_s) \text{ MeV}, \\ f_B^* &= 181(6)(stat)(18)(pert)(9)(disc)(13)(NRQCD)(+55)(a^{-1}) \text{ MeV}, \\ f_{B_s^*} &= 213(4)(stat)(21)(pert)(9)(disc)(15)(NRQCD)(+60)(a^{-1})(-4)(\kappa_s) \text{ MeV}. \end{aligned}$$

Adding the statistical and systematic errors in quadrature (errors 1–4), there is a combined uncertainty of 14% in the decay constants. This indicates a determination of  $f_B$  to around 10% is possible using an  $O(1/M)$  NRQCD action with clover light fermions. However, first of all the error due to the uncertainty in the lattice spacing ( $\sim 30\%$ ) must be significantly reduced. Conversely, for  $f_{B_s}/f_B$  and  $f_{B_s^*}/f_{B^*}$  most systematic errors cancel, and these quantities can be more easily determined accurately. We find

$$\begin{aligned} f_{B_s}/f_B &= 1.14(2)(stat)(-2)(\kappa_s), \\ f_{B_s^*}/f_{B^*} &= 1.14(2)(stat)(-2)(\kappa_s). \end{aligned}$$

We presented a detailed study of the heavy quark mass dependence of the decay constants. We find the steep dependence of the tree-level  $PS$  decay constant, for which  $C_{PS} \sim 2 \text{ GeV}$ , is dramatically reduced when the 1-loop terms are included;  $C_{PS} = 1-0 \text{ GeV}$  depending on  $q^*$ . We show how this occurs through the cancellation between the various 1-loop and tree-level current corrections as the individual terms vary with the heavy quark mass.

We have shown that simulating directly at the  $B$  with  $a^{-1}$  such that  $aM_0^b$  is in the region of 2 is advantageous. In particular, this value of  $aM_0$  sits in the window between large perturbative corrections for larger  $aM_0$  and significant contributions from higher orders in NRQCD for smaller  $aM_0$ . Nevertheless, the 1-loop matching factors should be checked by a nonperturbative determination; this is essential for a determination of the slope. Similarly, for the smaller meson masses studied here, higher orders in the NRQCD expansion should be considered. However, there are no indications that NRQCD is breaking down for the range of masses studied.

In addition, we present a tree-level analysis of the origin of the slope  $C_{PS}$ , and separate the contributions from the hyperfine and kinetic energy terms in the NRQCD action and the tree-level current correction. We find  $G_{kin} \sim 1.8$  GeV dominates  $C_{PS}$ , while the slope of the ratio  $f_{PS}\sqrt{M_{PS}}/f_V\sqrt{M_V}$ , related to  $G_{hyp}$  and  $G_{corr}$  is  $O(\Lambda_{QCD})$ , consistent with naive expectation from HQS. However, considering the results for the 1-loop corrections discussed previously (which are not suitable for a study of HQS),  $G_{kin}$  is likely to be reduced significantly by renormalisation and 1-loop corrections to  $G_{corr}$  are also likely to be large.

With this extensive analysis of the decay constants we are able to perform a detailed comparison of our results with those from the  $O(1/M^2)$  quenched simulation at  $\beta = 6.0$ . We find that  $f_B$  appears to be considerably larger at  $n_f = 2$  compared to that at  $n_f = 0$ . Clearly,  $f_B$  is a quantity which is sensitive to internal quark loops, and further work is needed to investigate the dependence of the decay constant on the mass and the number of flavours of sea quarks. We find the sensitivity to  $n_f$  cancels in the ratio  $f_{B_s}/f_B$ .

## VII. ACKNOWLEDGEMENTS

The computations were performed on the CM-2 at SCRI. We thank the HEMCGC collaboration for use of their configurations, and J. Hein and G. P. Lepage for useful discussions. This work was supported by PPARC under grant GR/L56343 and the U.S. DOE under grants DE-FG02-91ER40690, DE-FG05-85ER250000 and DE-FG05-96ER40979. We acknowledge support by the NATO under grant CRG 941259 and the EU under contract CHRX-CT92-0051. SC has been funded as a research fellow by the Royal Society of Edinburgh and the Alexander von Humboldt Foundation.

## VIII. APPENDIX

In this section we illustrate the fitting analysis and extraction of the masses and amplitudes of the heavy-light meson correlators. The fitting method is described in detail in reference [8], and since the data is of similar quality in terms of efficacy of the smearing functions etc. we only present additional fits not shown in [8] and [9].

### A. Spectrum

Considering the spectrum initially, the simplest quantities to extract are the  $^1S_0$  and  $^3S_1$  ground state energies,  $E(^1S_0)$  and  $E(^3S_1)$  respectively. A multiple exponential ‘vector’



fit was performed to the  $C(l, 1)$  and  $C(l, 2)$  correlators, where  $C(l, 1)$  ( $C(l, 2)$ ) denotes a correlator with the heavy quark smeared at the source with a hydrogen-like ground (first excited) state wavefunction and local at the sink. The operators inserted at the source and sink constructed from heavy and light quarks are given in table XIX.

An example of the quality and stability of the fits is shown in figure 11 for  $aM_0 = 1.0$  and  $\kappa_l = 0.1385$ . The ground state energy extracted from a single exponential fit ( $n_{exp} = 1$ ) in the range  $t_{min} > 12$  is in agreement with  $E(^1S_0)$  from a  $n_{exp} = 2$  fit for  $3 < t_{min} < 10$ , and we feel confident that we have minimal excited state contamination. The excited state energy is stable with  $t_{min}$ , however, a  $n_{exp} = 3$  fit is needed to confirm this state. Similar results are found for all  $M_0$  and  $\kappa_l$  and we chose a fitting range of 5 – 20 with  $n_{exp} = 2$  for both  $^1S_0$  and  $^3S_1$  mesons.

Tables XX and XXII detail the energies extracted. The results are chirally extrapolated to zero light quark mass and we find only linear dependence in  $1/\kappa_l$ ; figure 12 shows the chiral extrapolation of  $E_{sim}^{PS}$  for  $aM_0 = 1.0$ .

The hyperfine splittings,  $E(^3S_1) - E(^1S_0)$  and  $E(^2^3S_1) - E(^2^1S_0)$ , are calculated from the differences of 100 bootstrap samples of the  $n_{exp} = 2$  fits. In order to study the dependence of these and other splittings on the heavy quark mass, the meson mass ( $M_{PS}$ ) is calculated using the mass shifts,  $\Delta = M_{PS} - E(^1S_0)$ , obtained from heavy quarkonia dispersion behaviour, given in reference [8]. The mass shifts are given in table XX.

The singlet and triplet  $l = 1$  states,  $^1P_1$ ,  $^3P_1$ ,  $^3P_2$  and  $3P_0$ , were also computed for  $aM_0 = 1.0, 2.0$  and  $4.0$ . The corresponding operators used in the simulation are given in table XIX. As noted in [8] we cannot resolve the spin splittings between these states with the statistics available. Thus, we present the results for the  $^1P_1$  state and ignore the mixing with the  $^3P_1$  state. Figure 13 shows a  $n_{exp} = 1$  fit to the  $C(l, 2)$  correlator is stable as  $t_{min}$  is varied and we chose the fitting range 4 – 10 for all  $aM_0$  and  $\kappa_l$ . The ground and first excited state smearing functions did provide significantly different overlap with the lowest two states. However, since the signal died out around  $t \sim 10$  there were too many higher states contributing to enable a 1, 2 or 3 exponential fit to  $C(l, 1)$  and  $C(l, 2)$ . Table XXIV gives the results for different  $aM_0$  and  $\kappa_l$ .

In addition to the meson spectrum the  $J^P = \frac{1}{2}^+$  baryon containing one heavy quark,  $\Lambda_Q$ , was computed. The lattice operator,

$$\epsilon_{abc} \sum_{\vec{x}_1} Q_\alpha^a(\vec{x}_1) \sum_{\vec{x}_2} (q^b)^T(\vec{x}_2) C \gamma_5 \gamma_0 q^c(\vec{x}_2) \phi(|\vec{x}_1 - \vec{x}_2|) \quad (62)$$

has the correct quantum numbers for this particle, where  $a, b$  and  $c$  are the colour indices and  $\alpha$  is the spinor index.  $\phi$  represents the (hydrogen-like) smearing function and  $C$  is the charge conjugation matrix  $\gamma_0 \gamma_2$ . Figure 14 presents the energy of the ground state extracted from multi-exponential fits to  $C(l, 1)$  for  $aM_0$  and  $\kappa_l = 0.1385$ .  $E(\Lambda_Q)$  is stable with  $t_{min}$  for  $n_{exp} = 1$ . This is also the case when including another exponential in fitting to the same correlator. We found the fitting range 7 – 20 for the  $n = 1$  fit is sufficient for all  $aM_0$  and  $\kappa_l$ , and the corresponding values of the ground state energy are given in table XXV.

## B. Decay Constants

The zeroth order pseudoscalar and vector decay constants,  $f_{PS}^{(0)}\sqrt{M_{PS}}$  and  $f_V^{(0)}\sqrt{M_V}$  respectively, were extracted in the standard way from simultaneously fitting to the  $C(l, 1)$  and  $C(1, 1)$  correlators. The amplitudes of these correlators are related to the decay constant via:

$$C(l, 1) = Z_l Z_1 e^{-Et}, \quad (63)$$

$$C(1, 1) = Z_1^2 e^{-Et}. \quad (64)$$

where,

$$\sqrt{2}Z_l = f^{(0)}\sqrt{M}. \quad (65)$$

Note that the correction to the current is not included in  $C(l, 1)$ . The typical quality of the fits is illustrated in figure 15 for the  $PS$  meson. We found 7 – 20 to be the optimal fitting range for  $PS$  and  $V$  mesons for all  $aM_0$  and  $\kappa_l$ . The corresponding amplitudes obtained from 100 bootstrap samples of the fit parameters are presented in tables VI and VIII for the  $PS$  and  $V$  respectively. The results are extrapolated to zero light quark mass, an example of which is shown in figure 12 for the  $PS$  decay constant.

The tree-level corrections to the  $PS$  and  $V$  currents,  $f_{PS}^{(1)}\sqrt{M_{PS}}$  and  $f_V^{(1)}\sqrt{M_V}$  respectively, are obtained separately by computing the jackknife ratio of the correlator with the tree-level current correction operator inserted at the sink ( $C(l_{J(1)}, 1)$ ) with  $C(l, 1)$ ;  $J^{(1)}$  is given in equations 13 and 25 for the  $PS$  and  $V$  respectively. In the limit of large times this ratio tends to  $f^{(1)}\sqrt{M}/f^{(0)}\sqrt{M}$ . From figure 16 we see that 8 – 20 is a reasonable fitting range, and this was found to be optimal for all  $aM_0$  and  $\kappa_l$ . Tables VII and IX give the resulting tree-level corrections to the decay constant for the  $PS$  and  $V$  mesons respectively. The only 1-loop correction which must be calculated is  $f_V^{(3)}\sqrt{M_V}$ . This is obtained in the same way as the tree-level correction. The results are detailed in table X.

## REFERENCES

- [1] M. B. Wise, talk given at Les Houches Summer School in Theoretical Physics, Session 68: Probing the Standard Model of Particle Interactions, Les Houches, France, 28 Jul - 5 Sep 1997, CALT-68-2172, hep-ph/9805468. M. Neubert, *Int. J. Mod. Phys.* **A11** (1996) 4173. J. M. Flynn and C. T. Sachrajda, in “Buras, A.J. (ed.), Lindner, M. (ed.): Heavy flavours II” 402-452. C. Davies, in “Schladming 1997, Computing particle properties” 1-64.
- [2] A. Ali Khan et al, *Nucl. Phys.* **b(Proc. Suppl.) 73** (1999) 345 and in preparation.
- [3] A. Ali Khan et al, *Phys. Lett.* **B427** (1998) 132.
- [4] K. M. Bitar et al, *Phys. Rev.* **D46** (1992) 2169.
- [5] S. Collins et al, *Nucl. Phys. (Proc. Suppl.)* **60A** (1998) 34.
- [6] A. El-Khadra et al, *Phys. Rev* **D55** (1997) 3933.
- [7] G. P. Lepage et al, *Phys. Rev.* **D46**, 4052 (1992).
- [8] S. Collins et al, *Phys. Rev.* **D54** (1996) 5777.
- [9] S. Collins et al, *Phys. Rev.* **D55** (1997) 1630.
- [10] M. Lüscher et al, *Nucl. Phys.* **B491** (1997) 323.
- [11] H. Wittig, *Nucl. Phys.* **B(Proc. Suppl.) 63** (1998) 47.
- [12] K-I. Ishikawa et al, *Phys. Rev.* **D56** (1997) 7028.
- [13] R. Lewis and R. Woloshyn, JLAB-THY-98-05, hep-lat/9803004.
- [14] H. Trottier and G. P. Lepage, *Nucl. Phys.* **B(Proc. Suppl.) 63** (1998) 865.
- [15] C. Morningstar and J Shigemitsu, *Phys. Rev.* **D57** (1998) 6741.
- [16] C. Morningstar and J. Shigemitsu, *Nucl. Phys.* **b(Proc. Suppl.) 73** (1999) 345. C. Morningstar and J. Shigemitsu, *Phys. Rev.* **D59** (1999) 094504.
- [17] J. Shigemitsu, *Nucl. Phys. (Proc. Suppl.)* **60A** (1998) 134.
- [18] J. Hein et al, *Nucl. Phys.* **B(Proc. Suppl.) 63** (1998) 347.
- [19] K-I. Ishikawa et al., *Nucl. Phys.* **b(Proc. Suppl.) 73** (1999) 363.
- [20] A. Duncan et al, *Phys. Rev.* **D51** (1995) 5101.
- [21] A. Ukawa, *Nucl. Phys.* **B (Proc. Suppl.) 30** (1993) 3.
- [22] H. Hoerber, *Nucl. Phys.* **B (Proc. Suppl.) 63** (1998) 218.
- [23] C. T. H. Davies et al, *Phys. Rev.* **D58** (1998) 054505.
- [24] S. Gottlieb, results for finite volume effects on the  $\rho$  meson can be found on the web page ‘[http://physics.indiana.edu/~sg/lat96\\_spectrum.html](http://physics.indiana.edu/~sg/lat96_spectrum.html)’. This data was compiled for a talk given at 15th International Symposium on Lattice Field Theory (LATTICE 97), Edinburgh, Scotland, 22-27 Jul 1997, but the data was not included in the proceedings.
- [25] DELPHI Collaboration, Report No: DELPHI 96-93 CONF 22, contribution to ICHEP ’96.
- [26] Particle Data Group, C. Caso et al, *Eur. Phys. Journal* **C3** (1998) 1.
- [27] N. Isgur and M. Wise, *Phys. Lett.* **B66** (1991) 1130.
- [28] G. P. Lepage and P. B. Mackenzie, *Phys. Rev* **D48** (1993) 2250.
- [29] O. Hernandez and B. Hill, *Phys. Rev.* **D50** (1994) 495.
- [30] UKQCD Collaboration R. Baxter et al, *Phys. Rev.* **D49** 1594 (1994).
- [31] C. Bernard et al, *Phys. Rev.* **D49** (1994) 2536.
- [32] A. El-Khadra et al, *Phys. Rev.* **D58** (1998) 014506.
- [33] T. Onogi, *Nucl. Phys.* **B(Proc. Suppl.) 63** (1998) 59.

[34] MILC collaboration, C. Bernard et al, FSU-SCRI-98-65, hep-ph/9806412.

TABLES

TABLE I. The systematic errors expected to dominate the predictions of mass splittings and decay constants of the  $B$  meson.

Quantity	Dominant Errors	Size
$B^* - B$	Pert. correction to $c_B$	$O(\alpha_S(\Lambda_{QCD}/M)) \sim 10-30\%$
$B_s - B$	Determination of $\kappa_s$	$\sim 10\%$
	Light quark discretisation	$O((a\Lambda_{QCD})^2), O(\alpha(a\Lambda_{QCD})) < 5\%$
	Finite volume	$5\% ?$
$B(2S) - B(1S)$	Finite volume	$< 10\% ?$
$B^{**} - B$	Light quark discretisation	$O((a\Lambda_{QCD})^2), O(\alpha(a\Lambda_{QCD})) < 5\%$
$\Lambda_B - B$		
$f_B, f_{B^*}$	Light quark discretisation	$O((a\Lambda_{QCD})^2) < 5\%$
	Pert. matching factors	$O(\alpha^2) \sim 1-10\%$
	Truncation of NRQCD series	$O(1/M^2) \sim 6\%$
	Finite volume	$5\% ?$
$f_B/f_{B_s}$	Determination of $\kappa_s$	$\sim 2\%$

TABLE II. Values of the inverse lattice spacing in GeV as determined from light hadrons and heavy quarkonia [23] for this ensemble and a similar quenched ensemble at  $\beta^{n_f=0} = 6.0$  [23,3].

	$\rho$	$\Upsilon(1P - 1S)$	$\Upsilon(2S - 1S)$
$\beta^{n_f=2} = 5.6$	1.97(3)	2.44(7)	2.37(10)
$\beta^{n_f=0} = 6.0$	1.93(3)	2.59(5)	2.45(8)

TABLE III. Predictions for various mass splittings compared to experiment. The results are converted into physical units (MeV) using  $a^{-1} = 2.0$  GeV. The first error shown is statistical while the second is the estimate of the systematic errors which we expect to be dominant, as detailed in table I; the third indicates the change in the prediction if  $a^{-1} = 2.4$  GeV is used and includes the change due to the change in  $M_0^b$ . For  $B_s - B$  the systematic errors are split up between the light quark discretisation error and that due to the uncertainty in  $\kappa_s$ . The systematic error for the hyperfine splitting indicates the change in the central value if  $c_B$  is increased by 30%.

	$\beta^{n_f=2} = 5.6$	expt
$B^* - B$	20(12)(+6)(+6)	45.7(4)
$B_s^* - B_s$	26(8)(+10)(+9)	47(3)
$B_s - B$	98(8)(5)(-12)(+20)	90(2)
$B(2S) - B(1S)$	540(120)(23)(+110)	$\sim 580$
$B_s(2S) - B_s(1S)$	500(80)(20)(+100)	-
$B^*(2S) - B(2S)$	78(32)(10)(+22)	-
$B^{**} - B$	520(40)(20)(+110)	350–500
$\Lambda_b - B$	560(40)(22)(+110)	345(9)

TABLE IV. The coefficients of various spectral quantities, as determined from first order perturbation theory in  $1/M$ . The results are in physical units, GeV and  $\text{GeV}^2$  for  $C_0$  and  $C_1$  respectively, converted using  $a^{-1} = 2.0$  GeV. The hyperfine term has been ignored for the  $^1P_1$  state. Unless stated otherwise,  $\kappa_l = \kappa_c$ .

Quantity	Coefficient	Results	Expectation	Expt
$\bar{E}(2S) - \bar{E}(1S)$	$C_0 = \bar{\Lambda}_{2S} - \bar{\Lambda}_{1S}$	0.38(10)	$+\Lambda_{QCD}$	-
	$C_1 = \langle 2S   \mathcal{O}_{kin}   2S \rangle_{phys} - \langle 1S   \mathcal{O}_{kin}   1S \rangle_{phys}$	0.60(40)	+ve	-
$E(^3S_1)_{\kappa_s} - E(^1S_0)_{\kappa_s}$	$C_0 = 0$	0.002(8)	0	$\sim 0$
	$C_1 = \langle 1S   \mathcal{O}_{hyp}   1S \rangle_{\kappa_s}^{phys}$	0.08(4)	$+(\Lambda_{QCD})^2$	$\sim 0.28$
$E(^3S_1)_{\kappa_s} - E(^2^1S_0)_{\kappa_s}$	$C_0 = 0$	-0.02(2)	0	-
	$C_1 = \langle 2S   \mathcal{O}_{hyp}   2S \rangle_{\kappa_s}^{phys}$	0.56(28)	$+(\Lambda_{QCD})^2$	-
$\bar{E}(^1S_0)_{\kappa_s} - \bar{E}(^1S_0)_{\kappa_c}$	$C_0 = \bar{\Lambda}_{\kappa_s} - \bar{\Lambda}_{\kappa_c}$	0.106(10)		$\sim .085$
	$C_1 = \langle 1S   \mathcal{O}_{kin}   1S \rangle_{\kappa_s}^{phys} - \langle 1S   \mathcal{O}_{kin}   1S \rangle_{\kappa_c}^{phys}$	0.020(32)		$\sim 0.03$
$E(\Lambda_Q) - \bar{E}(1S)$	$C_0 = \bar{\Lambda}_{1/2^+} - \bar{\Lambda}$	0.58(4)	$\Lambda_{QCD}$	$\sim 0.36$
	$C_1 = \langle \frac{1}{2}^+   \mathcal{O}_{kin}   \frac{1}{2}^+ \rangle_{phys} + \langle \frac{1}{2}^+   \mathcal{O}_{hyp}   \frac{1}{2}^+ \rangle_{phys} - \langle 1S   \mathcal{O}_{kin}   1S \rangle_{phys}$	-0.12(8)		$\sim -0.1$
$E(^1P_1) - \bar{E}(1S)$	$C_0 = \bar{\Lambda}_{^1P_1} - \bar{\Lambda}$	0.40(2)	$\Lambda_{QCD}$	-
	$C_1 = \langle ^1P_1   \mathcal{O}_{kin}   ^1P_1 \rangle_{phys} - \langle 1S   \mathcal{O}_{kin}   1S \rangle_{phys}$	0.36(8)		-

TABLE V. Predictions for various mass splittings from this work and previous results on quenched configurations [2]. The experimental values are also included. The results in both cases are converted into physical units (MeV) using the scale from  $m_\rho$ , given in table II. The error shown is purely statistical, except for  $B_s - B$ , where the uncertainty in  $\kappa_s$  is shown. The central value for this splitting is set using  $\kappa_s$  from the  $K$  meson.

	$\beta^{n_f=0} = 6.0$	$\beta^{n_f=2} = 5.6$	expt
$B^* - B$	24(5)	20(12)	45.7(4)
$B_s^* - B_s$	27(3)	26(8)	47(3)
$B_s - B$	87(9)(+20)	98(8)(-12)	90(2)
$B(2S) - B(1S)$	602(86)	540(120)	$\sim 580$
$B_s(2S) - B_s(1S)$	559(55)	500(80)	-
$B^{**} - B$	474(32)	520(40)	350-500
$\Lambda_b - B$	388(68)	560(40)	345(9)

TABLE VI. The zeroth order decay amplitude of the  $PS$  meson,  $a^{3/2}f_{PS}^{(0)}\sqrt{M_{PS}}$ , for all  $aM_0$  and  $\kappa_l$ .

$aM_0$	0.1385	0.1393	0.1401	$\kappa_c$
0.8	0.203(3)	0.190(3)	0.176(6)	0.167(4)
1.0	0.214(3)	0.200(3)	0.185(6)	0.175(5)
1.2	0.221(4)	0.207(4)	0.191(6)	0.181(6)
1.7	0.236(4)	0.220(4)	0.203(6)	0.192(5)
2.0	0.243(4)	0.227(4)	0.210(7)	0.197(6)
3.0	0.262(4)	0.244(5)	0.227(7)	0.212(7)
3.5	0.268(4)	0.251(5)	0.234(5)	0.219(6)
4.0	0.274(4)	0.256(6)	0.243(8)	0.224(8)
7.0	0.295(5)	0.275(6)	0.270(19)	0.239(8)
10.0	0.309(6)	0.288(7)	0.278(26)	0.249(8)

TABLE VII. The tree-level correction to the  $PS$  current,  $a^{3/2}f_{PS}^{(1)}\sqrt{M_{PS}} = a^{3/2}f_{PS}^{(2)}\sqrt{M_{PS}}$ , for all  $aM_0$  and  $\kappa_l$ .

$aM_0$	0.1385	0.1393	0.1401	$\kappa_c$
0.8	-0.0520(10)	-0.0494(9)	-0.0462(17)	-0.0446(13)
1.0	-0.0467(9)	-0.0443(8)	-0.0414(15)	-0.0398(12)
1.2	-0.0422(9)	-0.0399(8)	-0.0372(13)	-0.0358(12)
1.7	-0.0340(7)	-0.0321(7)	-0.0299(10)	-0.0286(10)
2.0	-0.0308(5)	-0.0291(6)	-0.0271(10)	-0.0258(10)
3.0	-0.0234(4)	-0.0220(5)	-0.0207(7)	-0.0196(8)
3.5	-0.0209(4)	-0.0197(5)	-0.0185(4)	-0.0175(5)
4.0	-0.0189(4)	-0.0178(5)	-0.0170(6)	-0.0159(6)
7.0	-0.0120(2)	-0.0113(3)	-0.0112(9)	-0.0100(4)
10.0	-0.0089(2)	-0.0084(3)	-0.0082(8)	-0.0074(3)



TABLE VIII. The zeroth order decay amplitude of the  $V$  meson,  $a^{3/2}f_V^{(0)}\sqrt{M_V}$ , for all  $aM_0$  and  $\kappa_l$ .

$aM_0$	0.1385	0.1393	0.1401	$\kappa_c$
0.8	0.163(3)	0.152(3)	0.140(5)	0.131(4)
1.0	0.176(3)	0.164(3)	0.151(5)	0.142(4)
1.2	0.186(3)	0.174(3)	0.159(6)	0.150(4)
1.7	0.206(3)	0.191(4)	0.177(4)	0.165(5)
2.0	0.215(3)	0.201(4)	0.186(4)	0.173(5)
3.0	0.239(4)	0.223(5)	0.208(8)	0.194(6)
3.5	0.248(4)	0.232(5)	0.216(6)	0.202(7)
4.0	0.255(5)	0.239(6)	0.224(8)	0.209(7)
7.0	0.283(6)	0.264(6)	0.254(27)	0.230(10)
10.0	0.300(6)	0.279(7)	0.272(23)	0.241(9)

TABLE IX. The tree-level correction to the  $V$  current,  $a^{3/2}f_V^{(1)}\sqrt{M_V}$ , for all  $aM_0$  and  $\kappa_l$ .

$aM_0$	0.1385	0.1393	0.1401	$\kappa_c$
0.8	0.0136(3)	0.0128(3)	0.0119(5)	0.0114(5)
1.0	0.0126(3)	0.0119(3)	0.0111(5)	0.0106(4)
1.2	0.0117(3)	0.0110(3)	0.0102(4)	0.0097(3)
1.7	0.0098(2)	0.0092(2)	0.0086(3)	0.0082(3)
2.0	0.0090(1)	0.0085(2)	0.0079(3)	0.0075(3)
3.0	0.0071(1)	0.0067(2)	0.0063(3)	0.0060(2)
3.5	0.0064(1)	0.0061(2)	0.0057(2)	0.0054(2)
4.0	0.0059(1)	0.0055(2)	0.0052(2)	0.0050(2)
7.0	0.0038(1)	0.0036(1)	0.0035(4)	0.0032(1)
10.0	0.0029(1)	0.0027(1)	0.0027(2)	0.0024(1)

TABLE X. The one-loop correction to the  $V$  current,  $a^{3/2} f_V^{(3)} \sqrt{M_V} = a^{3/2} f_V^{(4)} \sqrt{M_V}$ , for all  $aM_0$  and  $\kappa_l$ .

$aM_0$	0.1385	0.1393	0.1401	$\kappa_c$
0.8	-0.0164(3)	-0.0154(3)	-0.0144(5)	-0.0136(6)
1.0	-0.0144(3)	-0.0136(3)	-0.0126(5)	-0.0119(4)
1.2	-0.0129(3)	-0.0121(3)	-0.0112(4)	-0.0107(4)
1.7	-0.0103(2)	-0.0097(2)	-0.0091(3)	-0.0086(3)
2.0	-0.0094(1)	-0.0088(2)	-0.0082(3)	-0.0078(3)
3.0	-0.0072(1)	-0.0068(2)	-0.0064(3)	-0.0061(2)
3.5	-0.0065(1)	-0.0061(2)	-0.0058(2)	-0.0055(2)
4.0	-0.0059(1)	-0.0056(2)	-0.0053(2)	-0.0050(2)
7.0	-0.0038(1)	-0.0036(1)	-0.0035(4)	-0.0032(1)
10.0	-0.0029(1)	-0.0027(1)	-0.0027(2)	-0.0024(1)

TABLE XI. The tree-level and renormalised  $PS$  decay constants in lattice units,  $a^{3/2} f_{PS} \sqrt{M_{PS}}$ , for all  $aM_0$  and  $\kappa_l = \kappa_c$ .  $aM_0$  has been used for the argument of the logarithms appearing in the matching coefficients.

$aM_0$	tree-level	$q^* = \pi$	$q^* = 1.0$
0.8	0.122(3)	0.121(3)	0.120(3)
1.0	0.135(4)	0.130(4)	0.126(3)
1.2	0.145(5)	0.137(4)	0.132(4)
1.7	0.163(5)	0.150(4)	0.141(3)
2.0	0.172(5)	0.155(4)	0.145(4)
3.0	0.192(5)	0.169(5)	0.154(5)
3.5	0.202(5)	0.175(5)	0.158(4)
4.0	0.208(7)	0.179(6)	0.161(5)
7.0	0.229(8)	0.195(6)	0.174(5)
10.0	0.242(9)	0.206(7)	0.184(6)

TABLE XII. The tree-level and renormalised  $V$  decay constants in lattice units,  $a^{3/2} f_V \sqrt{M_V}$ , for all  $aM_0$  and  $\kappa_l = \kappa_c$ .  $aM_0$  has been used for the argument of the logarithms appearing in the matching coefficients.

$aM_0$	tree-level	$q^* = \pi$	$q^* = 1.0$
0.8	0.143(4)	0.134(4)	0.128(4)
1.0	0.152(4)	0.139(4)	0.131(4)
1.2	0.159(5)	0.143(4)	0.134(4)
1.7	0.173(5)	0.152(5)	0.139(4)
2.0	0.181(6)	0.156(5)	0.141(4)
3.0	0.200(6)	0.168(5)	0.148(5)
3.5	0.207(7)	0.173(6)	0.151(6)
4.0	0.214(8)	0.177(6)	0.154(6)
7.0	0.232(9)	0.190(8)	0.164(7)
10.0	0.244(9)	0.199(7)	0.170(6)

TABLE XIII. The corrections to the zeroth order pseudoscalar and vector matrix elements expressed as a ratio to  $\langle J^{(0)} \rangle$ . The order at which each correction contributes is indicated.  $aq^* = 1.0$  and  $aM_0 = 2.0$ , which is close to the bare  $b$  quark mass for  $a^{-1} = 2.0$  GeV. Note that  $\zeta_A$  and  $\zeta_V$  are set to zero. The statistical errors are less than 1%.

	$\frac{\langle J^{(1)} \rangle}{\langle J^{(0)} \rangle}$	$\alpha\rho_0$	$\frac{\alpha\rho_1 \langle J^{(1)} \rangle}{\langle J^{(0)} \rangle}$	$\frac{\alpha\rho_2 \langle J^{(2)} \rangle}{\langle J^{(0)} \rangle} + \frac{\alpha \langle J^{disc} \rangle}{\langle J^{(0)} \rangle}$	$\frac{C_3 \langle J^{(3)} \rangle}{\langle J^{(0)} \rangle}$	$\frac{C_4 \langle J^{(4)} \rangle}{\langle J^{(0)} \rangle}$
	$O(1/M)$	$O(\alpha)$	$O(\alpha/M)$	$O(\alpha/M) + O(a\alpha)$	$O(\alpha/M)$	$O(\alpha/M)$
$f_{PS} \sqrt{M_{PS}}$	-13	-9	+1	-7	-	-
$f_V \sqrt{M_V}$	+4	-14	+1	-6	-1	-1

TABLE XIV. The pseudoscalar and vector decay constants in MeV, calculated with and without renormalisation and converted to physical units using  $a^{-1} = 2.0$  and  $2.4$  GeV. Note that  $aM_0^b = 2.0$  for  $a^{-1} = 2.0$  GeV, while  $aM_0^b = 1.8$  for  $a^{-1} = 2.4$  GeV. Statistical errors, only, are shown except for those involving  $f_{B_s}$  and  $f_{B_s^*}$ , where the error due to the uncertainty in  $\kappa_s$  is also given.

	$a^{-1}$ GeV	tree-level	$q^* = \pi$	$q^* = 1.0$
$f_B$	2.0	217(6)	192(5)	180(5)
	2.4	269(8)	244(8)	231(8)
$f_{B_s}$	2.0	247(5)(-5)	222(2)(-5)	208(2)(-5)
	2.4	310(6)(-6)	284(4)(-6)	266(4)(-6)
$f_{B^*}$	2.0	223(6)	189(6)	173(5)
	2.4	280(8)	248(8)	224(6)
$f_{B_s^*}$	2.0	256(4)(-3)	224(4)(-4)	202(4)(-4)
	2.4	323(6)(-6)	285(5)(-7)	261(5)(-5)
$f_{B_s}/f_B$	-	1.14(2)(-2)	1.14(2)(-2)	1.14(2)(-2)
$f_{B_s^*}/f_{B^*}$	-	1.14(2)(-2)	1.14(2)(-2)	1.14(2)(-2)

TABLE XV. The dependence of the  $O(1/M)$  slope of  $a^{3/2}f\sqrt{M_{PS}}$  on the light quark mass in lattice units.

$\kappa_l$	$aC_1/C_0$
0.1385	1.7(5)
0.1393	1.0(4)
0.1401	1.1(3)
$\kappa_c$	1.1(3)

TABLE XVI. The slope of  $a^{3/2}f\sqrt{M_{PS}}$  in lattice units at tree-level and when renormalisation is included.

	$a^{3/2}C_0$	$a^{5/2}C_1$	$aC_1/C_0$
tree-level	0.27(1)	-0.3(1)	-1.1(3)
$q^* = \pi$	0.192(8)	-0.09(2)	-0.5(1)
$q^* = 1.0$	0.150(6)	-0.00(2)	-0.0(1)

TABLE XVII. The  $O(1/M)$  slope found for various combinations of the tree-level  $PS$  and  $V$  decay constants in lattice units.  $\kappa_l = \kappa_c$ .

Quantity	$aC_1/C_0$	Results
$f_{PS}\sqrt{M_{PS}}$	$G_{kin} + 6G_{hyp} + G_{corr}/2$	-1.1(3)
$f\sqrt{M}$	$G_{kin}$	-0.9(3)
$\frac{f_{PS}^{(0)}\sqrt{M_{PS}}}{f_V^{(0)}\sqrt{M_V}}$	$8G_{hyp}$	0.36(3)
$\frac{f_{PS}\sqrt{M_{PS}}}{f_V\sqrt{M_V}}$	$8G_{hyp} + 2G_{corr}/3$	-0.14(4)
Quantity	$aC_0$	Results
$\frac{2M_0 f_{PS}^{(1)}\sqrt{M_{PS}}}{f_{PS}^{(0)}\sqrt{M_{PS}}}$	$-G_{corr}$	-0.62(1)

TABLE XVIII. A comparison of the decay constants of the  $B$  and  $B_s$  mesons from this work and those on quenched configurations at  $\beta^{n_f=0} = 6.0$  [3]. The results have been converted into physical units (MeV) using  $a^{-1}$  from  $m_\rho$ . The errors are purely statistical, with the exception of  $f_{B_s}/f_B$  where the second error comes from the uncertainty in  $\kappa_s$ . Note that the  $O(1/M^2)$  current corrections included in reference [3] have been omitted from the quenched results in order to better compare with the  $n_f = 2$  results.

		$\beta^{n_f=0} = 6.0$	$\beta^{n_f=2} = 5.6$
$f_B$	$q^* = 1.0$	145(10)	180(5)
	$q^* = \pi$	154(10)	192(5)
	tree-level	176(11)	217(6)
$f_{B_s}$	$q^* = 1.0$	175(6)(+7)	208(2)(-4)
	$q^* = \pi$	186(6)(+7)	222(2)(-4)
	tree-level	205(6)(+7)	247(2)(-4)
$f_{B_s}/f_B$		1.20(4)(+4)	1.14(2)(-2)

TABLE XIX. The operators and corresponding quantum numbers used for the computation of the spectrum of the heavy-light mesons.

$^{2S+1}L_J (J^{PC})$	$q^\dagger \Gamma Q$
$^1S_0 (0^{-+})$	$q^\dagger \hat{I} Q$
$^3S_1 (1^{--})$	$q^\dagger \sigma_i Q$
$^1P_1 (1^{+-})$	$q^\dagger \Delta_i Q$
$^3P_0 (0^{++})$	$q^\dagger \sum_j \Delta_j \sigma_j Q$
$^3P_1 (1^{++})$	$q^\dagger (\Delta_i \sigma_j - \Delta_j \sigma_i) Q$
$^3P_2 (2^{++})$	$q^\dagger (\Delta_i \sigma_i - \Delta_j \sigma_j) Q$
	$q^\dagger (\Delta_i \sigma_j + \Delta_j \sigma_i) Q \quad (i \neq j)$

TABLE XX. The ground state pseudoscalar meson energies,  $aE(^1S_0)$ , extracted from  $n_{exp} = 2$  fits to  $C(l, 1)$  and  $C(l, 2)$  correlators. The mass shift needed to convert the simulation energies to the meson mass is also given.

$aM_0$	$\Delta$	0.1385	0.1393	0.1401	$\kappa_c$
0.8	0.89(2)	0.420(4)	0.395(4)	0.367(7)	0.347(7)
1.0	1.09(3)	0.465(4)	0.440(5)	0.412(8)	0.394(8)
1.2	1.27(2)	0.492(4)	0.467(5)	0.439(8)	0.421(9)
1.7	1.76(2)	0.524(5)	0.500(5)	0.473(8)	0.453(9)
2.0	2.07(2)	0.534(5)	0.509(5)	0.483(8)	0.463(10)
3.0	2.58(2)	0.548(5)	0.524(6)	0.499(9)	0.478(7)
3.5	3.10(3)	0.551(5)	0.528(6)	0.503(9)	0.483(9)
4.0	3.64(3)	0.553(5)	0.530(7)	0.507(9)	0.486(9)
7.0	6.61(12)	0.558(7)	0.536(7)	0.515(10)	0.492(10)
10.0	9.43(22)	0.560(8)	0.536(8)	0.515(11)	0.491(12)

TABLE XXI. The first excited state pseudoscalar meson energies,  $aE(2^1S_0)$ , extracted from  $n_{exp} = 2$  fits to  $C(l, 1)$  and  $C(l, 2)$  correlators.

$aM_0$	0.1385	0.1393	0.1401	$\kappa_c$
0.8	0.70(5)	0.68(5)	0.68(6)	0.68(8)
1.0	0.73(4)	0.72(5)	0.71(5)	0.70(7)
1.2	0.75(3)	0.74(4)	0.72(5)	0.71(6)
1.7	0.77(3)	0.76(4)	0.74(5)	0.73(6)
2.0	0.78(3)	0.77(4)	0.74(5)	0.73(5)
3.0	0.78(3)	0.77(3)	0.74(4)	0.73(5)
3.5	0.78(3)	0.76(3)	0.74(5)	0.73(5)
4.0	0.77(3)	0.76(3)	0.74(4)	0.73(5)
7.0	0.76(3)	0.75(3)	0.75(4)	0.73(5)
10.0	0.74(3)	0.73(3)	0.73(5)	0.72(5)

TABLE XXII. The ground state vector meson energies,  $aE(3^1S_1)$ , extracted from  $n_{exp} = 2$  fits to  $C(l, 1)$  and  $C(l, 2)$  correlators.

$aM_0$	0.1385	0.1393	0.1401	$\kappa_c$
0.8	0.448(4)	0.422(5)	0.391(8)	0.372(9)
1.0	0.490(4)	0.463(5)	0.432(9)	0.415(9)
1.2	0.513(4)	0.487(6)	0.456(9)	0.440(9)
1.7	0.541(4)	0.515(6)	0.485(9)	0.470(9)
2.0	0.548(4)	0.523(5)	0.493(9)	0.477(8)
3.0	0.558(4)	0.534(5)	0.507(9)	0.488(8)
3.5	0.560(5)	0.536(5)	0.510(8)	0.490(7)
4.0	0.561(5)	0.537(5)	0.512(8)	0.492(8)
7.0	0.564(6)	0.540(7)	0.518(11)	0.494(9)
10.0	0.565(10)	0.541(9)	0.519(12)	0.495(13)

TABLE XXIII. The first excited state vector meson energies,  $aE(2^3S_1)$ , extracted from  $n_{exp} = 2$  fits to  $C(l, 1)$  and  $C(l, 2)$  correlators.

$aM_0$	0.1385	0.1393	0.1401	$\kappa_c$
0.8	0.75(5)	0.74(6)	0.71(6)	0.69(7)
1.0	0.78(5)	0.77(6)	0.74(6)	0.72(7)
1.2	0.80(4)	0.79(5)	0.75(5)	0.72(6)
1.7	0.81(4)	0.81(4)	0.76(5)	0.75(6)
2.0	0.82(3)	0.81(4)	0.76(5)	0.73(6)
3.0	0.81(3)	0.80(4)	0.76(5)	0.74(6)
3.5	0.80(3)	0.79(4)	0.76(4)	0.74(5)
4.0	0.80(3)	0.79(4)	0.76(4)	0.75(5)
7.0	0.77(3)	0.76(3)	0.75(4)	0.75(5)
10.0	0.74(3)	0.74(4)	0.74(4)	0.73(5)

TABLE XXIV. The ground state energy of the  $^1P_1$  state,  $aE(^1P_1)$ , for various  $aM_0$  and all  $\kappa_l$ .

$aM_0$	0.1385	0.1393	0.1401	$\kappa_c$
1.0	0.79(1)	0.77(1)	0.75(1)	0.74(1)
2.0	0.78(1)	0.76(1)	0.75(1)	0.74(1)
4.0	0.76(1)	0.75(1)	0.74(1)	0.71(1)

TABLE XXV. The ground state energy of the  $\Lambda_Q$ ,  $aE(\Lambda_Q)$ , extracted from  $n_{exp} = 1$  fits to  $C(l, 1)$  for all  $aM_0$  and  $\kappa_l$ .

$aM_0$	0.1385	0.1393	0.1401	$\kappa_c$
0.8	0.783(9)	0.727(13)	0.669(17)	0.621(20)
1.0	0.826(10)	0.773(13)	0.716(17)	0.671(18)
1.2	0.851(10)	0.799(12)	0.744(17)	0.701(17)
1.7	0.880(9)	0.832(11)	0.779(17)	0.739(18)
2.0	0.889(9)	0.841(10)	0.789(19)	0.751(18)
3.0	0.902(9)	0.858(10)	0.804(17)	0.772(18)
3.5	0.905(9)	0.862(10)	0.808(18)	0.778(18)
4.0	0.907(9)	0.865(12)	0.811(19)	0.782(17)
7.0	0.893(17)	0.873(13)	0.821(18)	0.801(28)
10.0	0.886(23)	0.878(12)	0.828(24)	0.819(26)



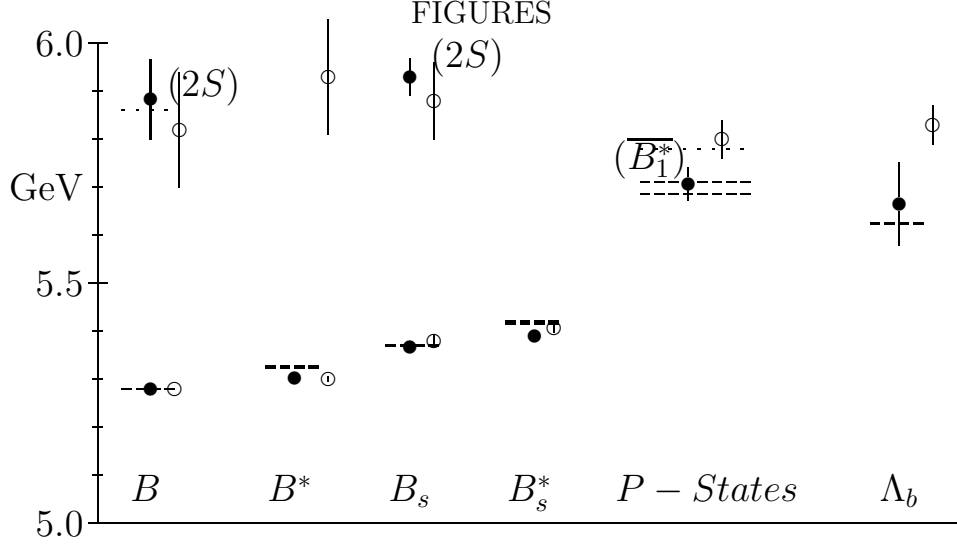


FIG. 1. The lower lying  $B$  spectrum and  $\Lambda_b$ . The open circles denote our results. The dashed lines denote the upper and lower bounds on the experimental results. The dotted lines indicate preliminary experimental signals. For the  $P$  states the dashed and dotted lines represent the  $B^{(*)}\pi$  and the narrow  $B\pi\pi$  resonance respectively. The errors shown are purely statistical. The filled circles represent preliminary results from a quenched simulation at  $\beta^{m_f=0} = 6.0$  [2]. All results are converted to physical units using the scale from  $m_\rho$ , given in table II.

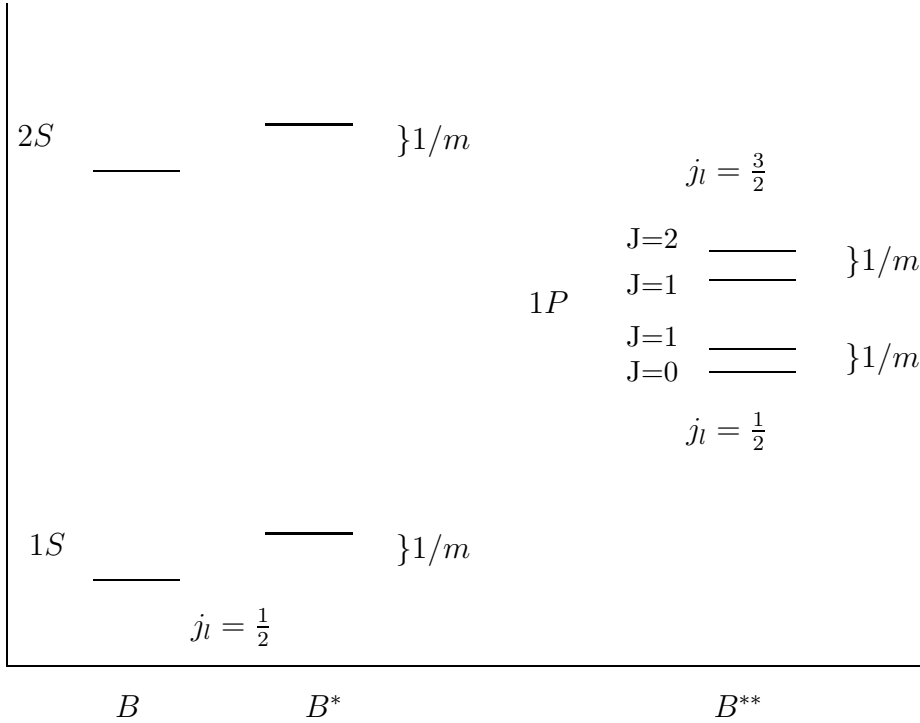


FIG. 2. The theoretical prediction for the structure of the  $B$  spectrum [27].  $j_l$  and  $J$  denote the total spin of the light quark and the heavy-light meson respectively.

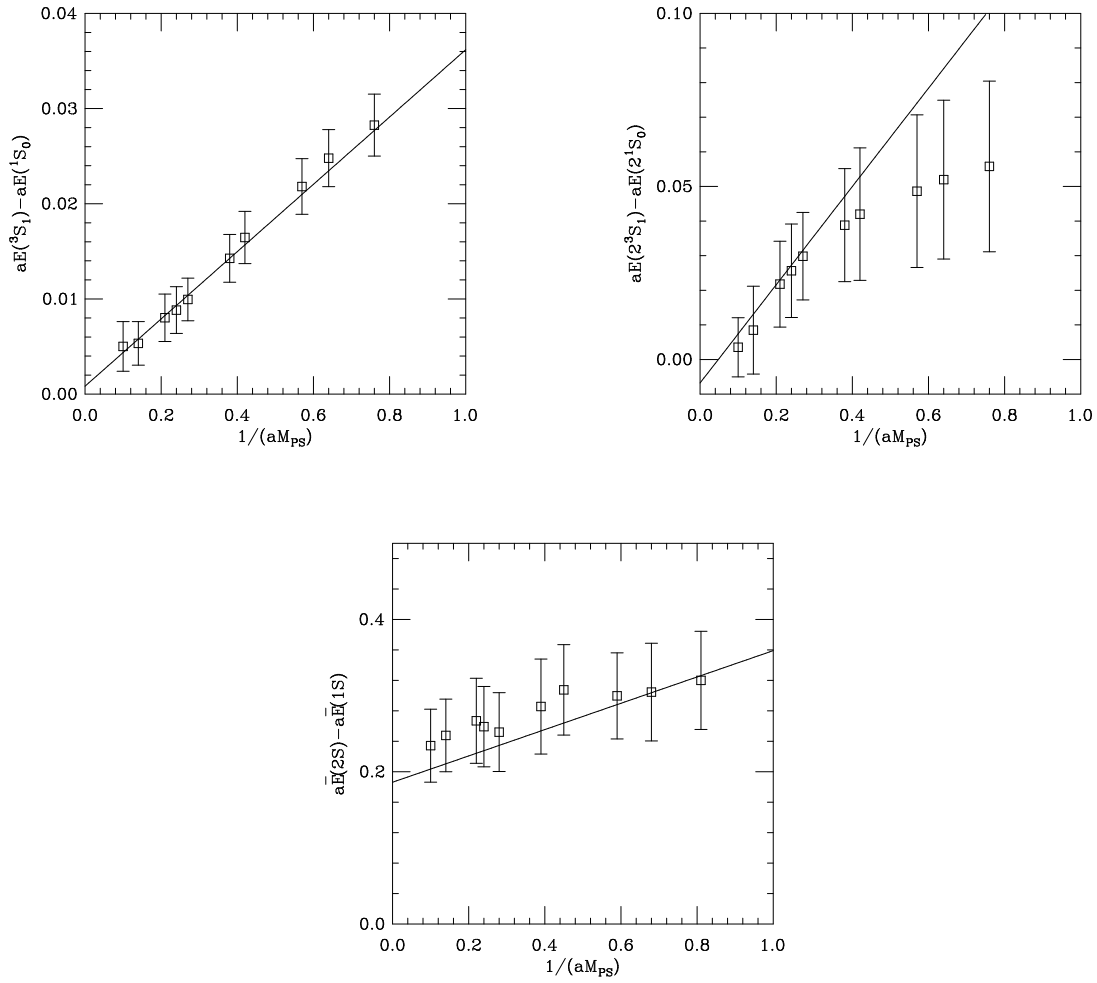


FIG. 3. The dependence of the mass splittings of the ground and first excited state  $PS$  and  $V$  mesons with the inverse pseudoscalar meson mass in lattice units.  $\kappa_l = \kappa_c$  for the  $\bar{E}(2S) - \bar{E}(1S)$  splitting, while  $\kappa_l = 0.1385$  for the  $1S$  and  $2S$  hyperfine splittings.

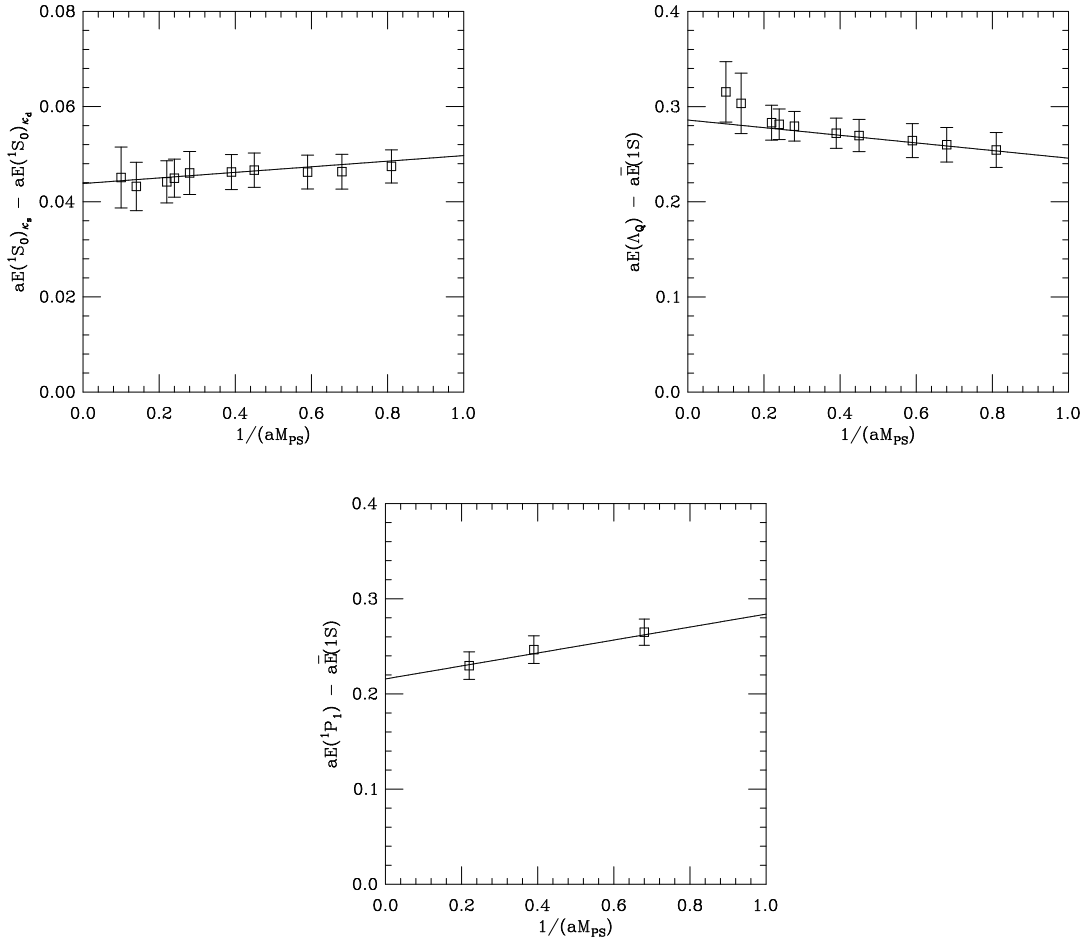


FIG. 4. The dependence of the  $E(^1S_0)_{\kappa_s} - E(^1S_0)_{\kappa_d}$ ,  $E(\Lambda_Q) - \bar{E}(1S)$  and  $E(1P) - E(1S)$  splittings on  $1/(aM_{PS})$  in lattice units, where  $\kappa_l = \kappa_c$ .

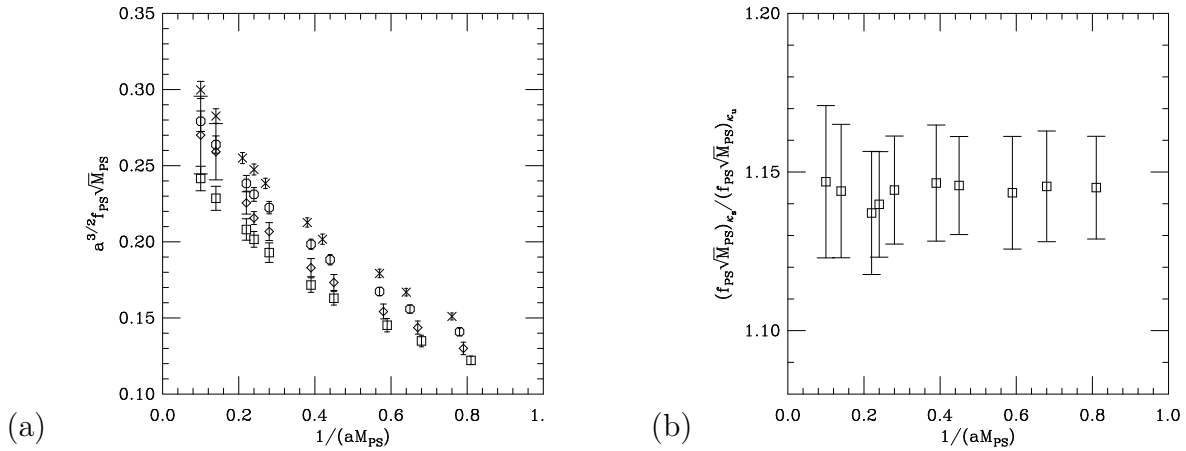


FIG. 5. (a) shows the tree-level  $a^{3/2} f_{PS} \sqrt{M_{PS}}$  for the three values of  $\kappa_l = 0.1385$  (crosses), 0.1393 (octagons) and 0.1401 (diamonds), and extrapolated to the chiral limit (squares) as a function of  $1/(aM_{PS})$ . (b) shows the heavy quark mass dependence of the ratio of  $(f_{PS} \sqrt{M_{PS}})_{\kappa_s}$  to  $(f_{PS} \sqrt{M_{PS}})_{\kappa_c}$ , where  $\kappa_s$  is fixed using the  $K$  meson.

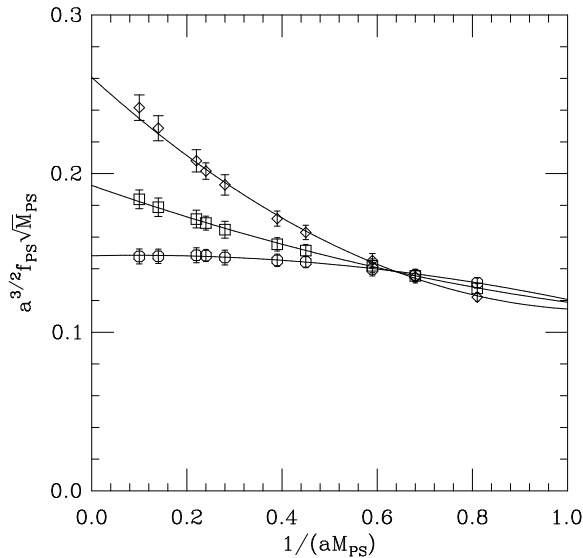


FIG. 6. The pseudoscalar decay constant in lattice units fully consistent to  $O(\alpha/M)$  as a function of  $1/(aM_{PS})$ . The results shown as circles are obtained using  $aq^* = 1.0$  for the renormalisation factors, while the squares use  $aq^* = \pi$ ; the tree-level results are also shown as diamonds.  $aM_0^b = 2.1$ , for  $a^{-1} = 2.0$  GeV, has been used for the argument of the logarithms appearing in the matching coefficients, for all  $aM_0$ . The results are for  $\kappa_l = \kappa_c$ .

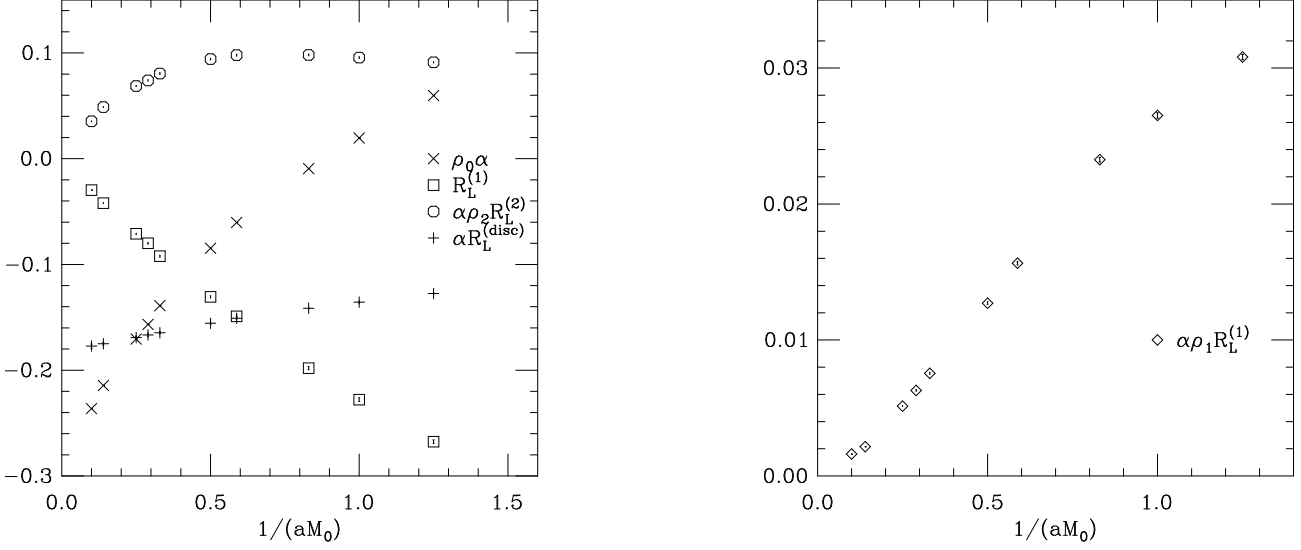


FIG. 7. The ratio of individual tree-level and 1-loop current corrections to the zeroth order  $PS$  decay constant,  $f^{(0)}\sqrt{M_{PS}}$ , as a function of  $1/(aM_0)$ .  $R_L^{(i)} = \langle J_L^{(i)} \rangle / \langle J_L^{(0)} \rangle$ .  $\kappa_l = \kappa_c$  and  $aq^* = 1.0$ .  $aM_0 = aM_0^b$  has been used for the argument of the logarithms appearing in the matching coefficients.

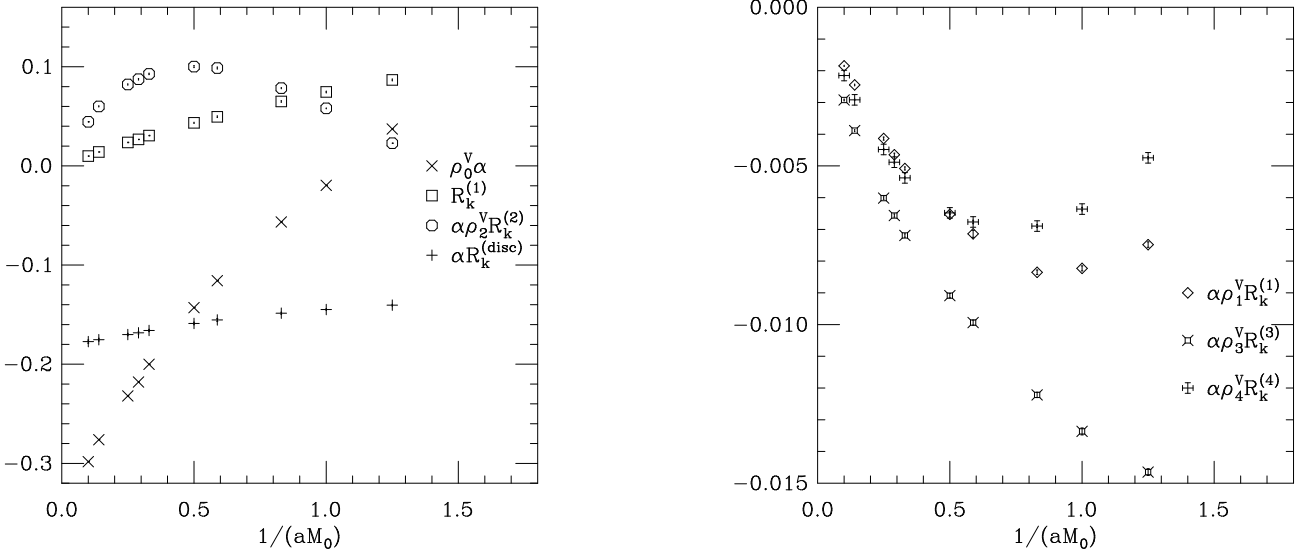


FIG. 8. The individual tree-level and 1-loop current corrections to the zeroth order  $V$  decay constant,  $f_V^{(0)}\sqrt{M_{PS}}$  as a function of  $1/(aM_0)$ .  $R_k^{(i)} = \langle J_k^{(i)} \rangle / \langle J_k^{(0)} \rangle$ .  $\kappa_l = \kappa_c$  and  $aq^* = 1.0$ .  $aM_0 = aM_0^b$  has been used for the argument of the logarithms appearing in the matching coefficients.

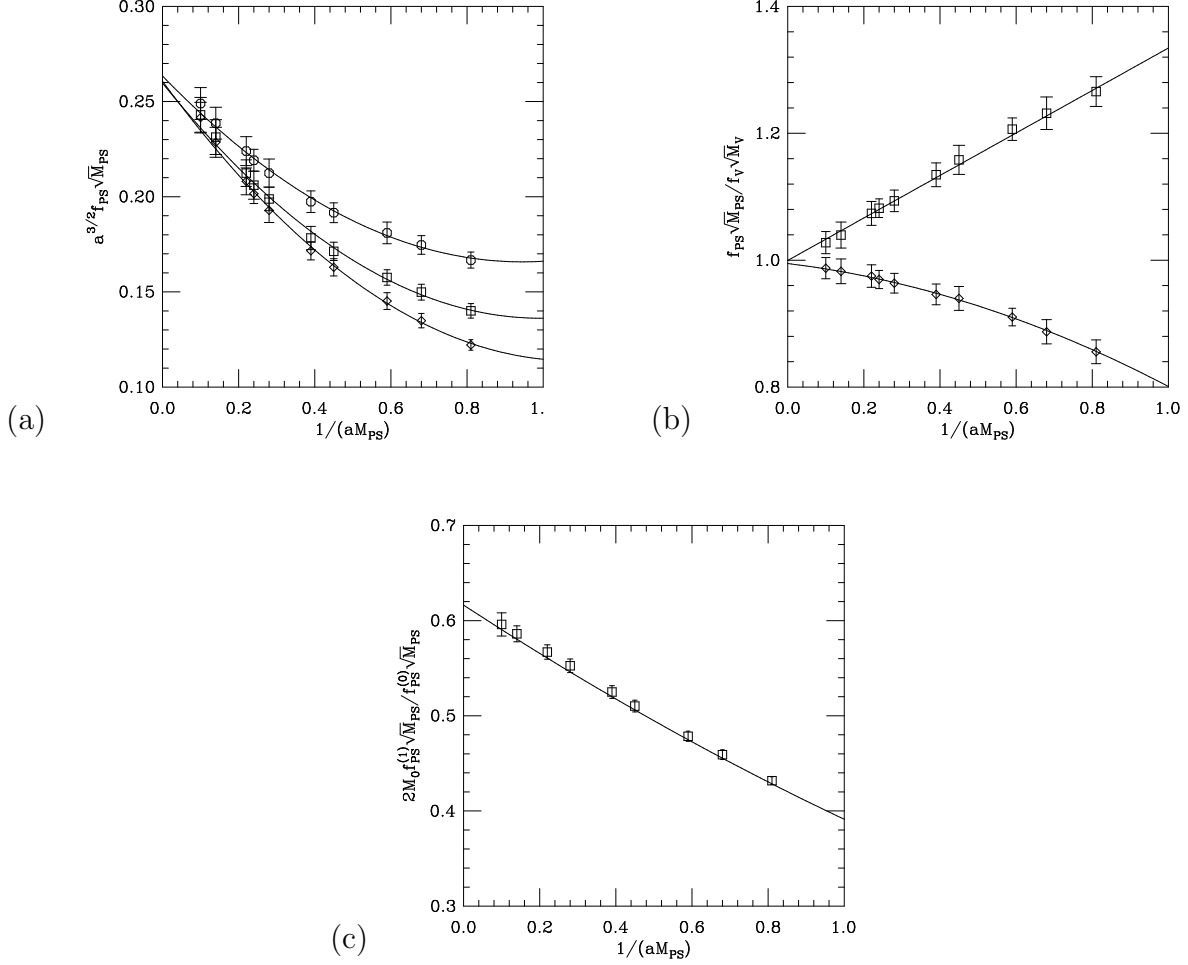


FIG. 9. Heavy quark dependence of various combinations of the tree-level  $PS$  and  $V$  decay constants in lattice units for  $\kappa_l = \kappa_c$ . (a) presents  $f \sqrt{M_{PS}}$  (diamonds),  $f^{(0)} \sqrt{M_{PS}}$  (octagons) and the spin-average of the  $PS$  and  $V$  decay constants (squares). (b) shows the ratio of the  $PS$  to the  $V$  tree-level decay constant with (diamonds) and without (squares) the  $O(1/M)$  current corrections. (c) gives the contribution to the slope of the decay constants from the  $O(1/M)$  current correction.

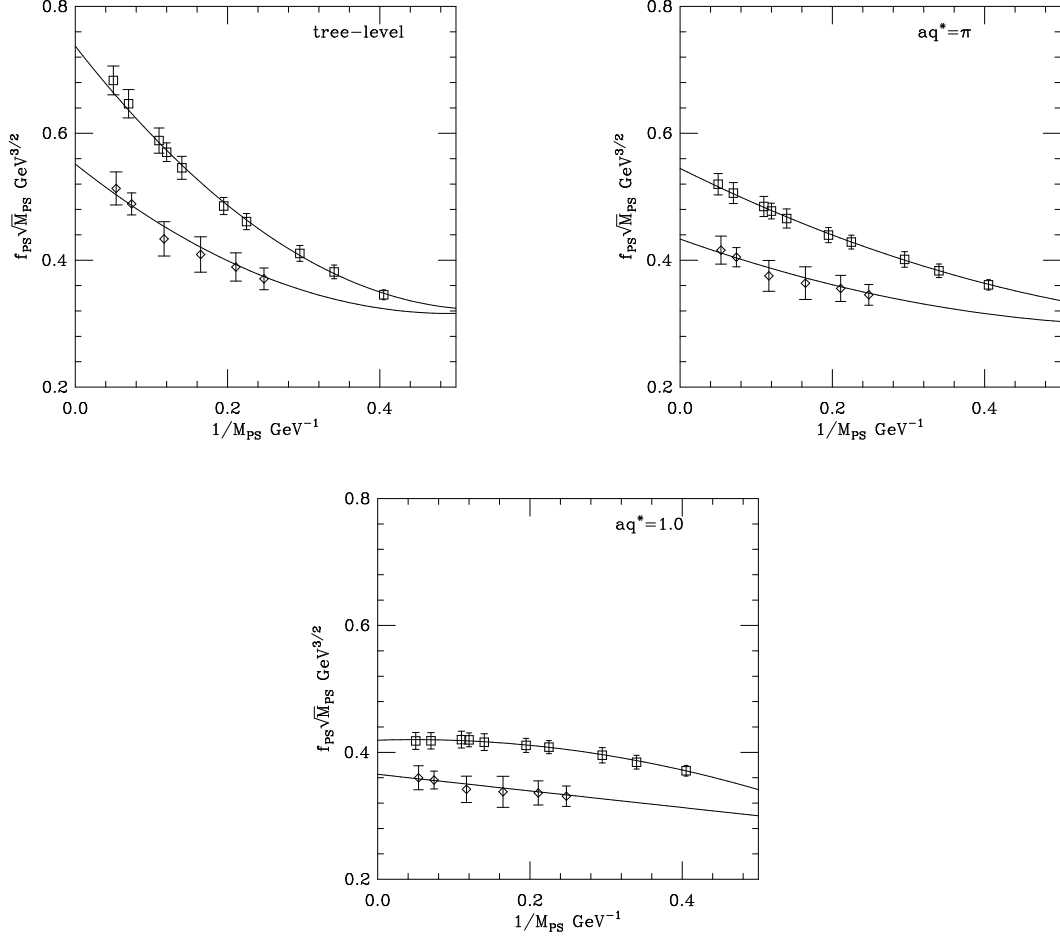


FIG. 10. The renormalised pseudoscalar decay constant as a function of  $1/M_{PS}$  in physical units for  $\beta_f^{n_f=0} = 6.0$  (diamonds  $1/M^2$ ) and  $\beta_f^{n_f=2} = 5.6$  (squares) for tree-level and 1-loop for  $q^* = \pi$  and  $q^* = 1.0$ .  $aM_0^b$  has been used for the argument of the logarithms appearing in the matching coefficients.

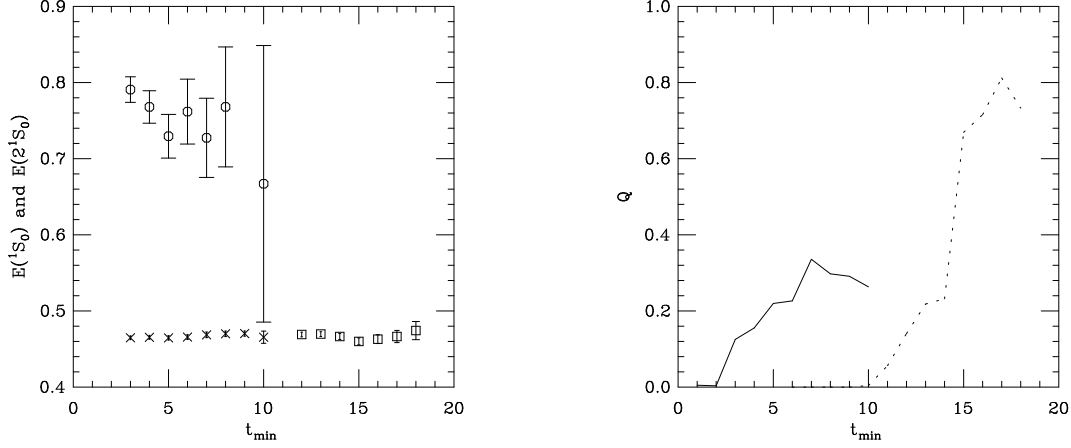


FIG. 11. The ground and first excited state energies extracted as a function of  $t_{min}$  from a vector fit to the  $C(l, 1)$  and  $C(l, 2)$  pseudoscalar correlators for  $aM_0 = 1.0$  and  $\kappa_l = 0.1385$ ;  $t_{max}$  is fixed to 20.  $E(1S_0)$  is shown as squares (crosses) for a one (two) exponential fit and  $E(2S_0)$  as circles for the two exponential fit. The quality of fit parameter,  $Q$ , is also shown as a dotted and solid line for a one and two exponential fit respectively, where  $Q > 0.1$  defines a 'good' fit.

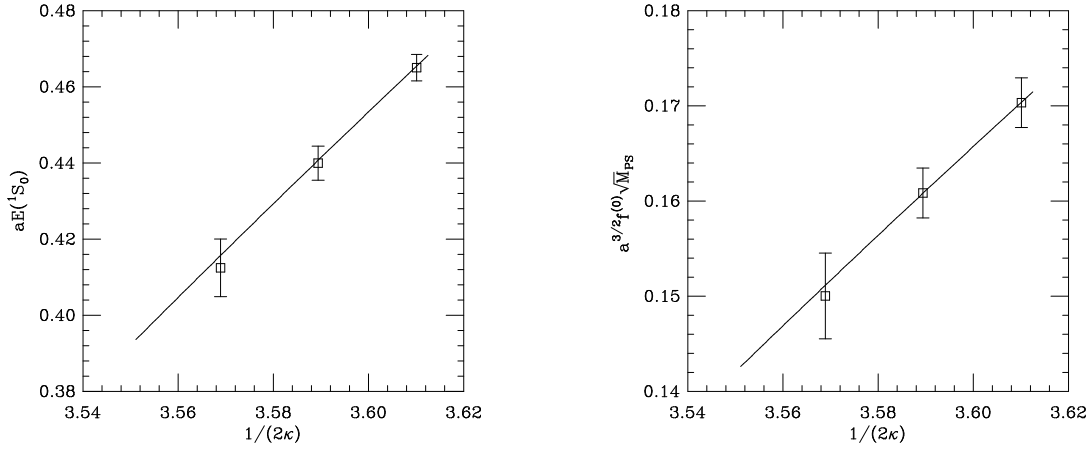


FIG. 12. The chiral extrapolation of  $aE(1S_0)$  and  $a^{3/2}f^{(0)}\sqrt{M_{PS}}$  in  $1/\kappa$  for  $aM_0 = 1.0$ .



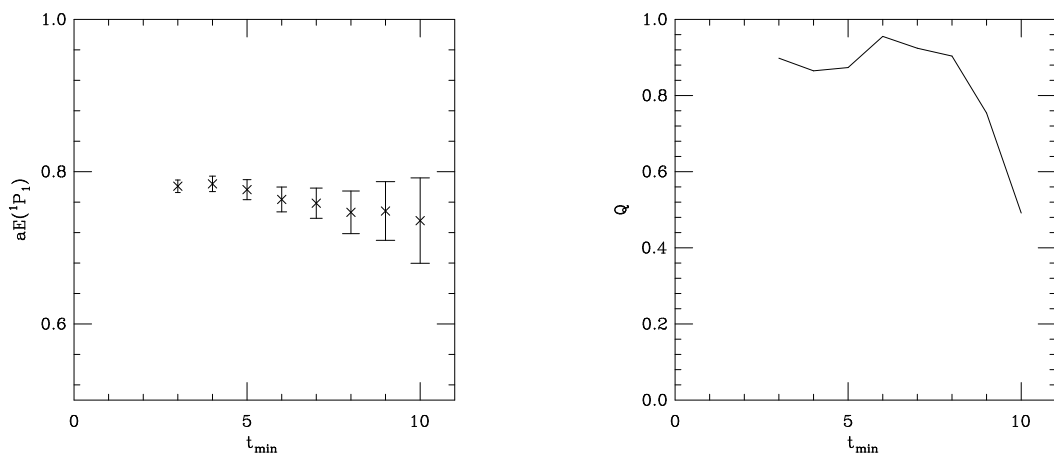


FIG. 13. The ground state energy of the  $^1P_1$  state extracted from a  $n_{exp} = 1$  fit to  $C(l, 2)$  as a function of  $t_{min}$  for  $aM_0 = 1.0$  and  $\kappa_l = 0.1385$ ;  $t_{max} = 10$ . The corresponding values of  $Q$  are also shown.

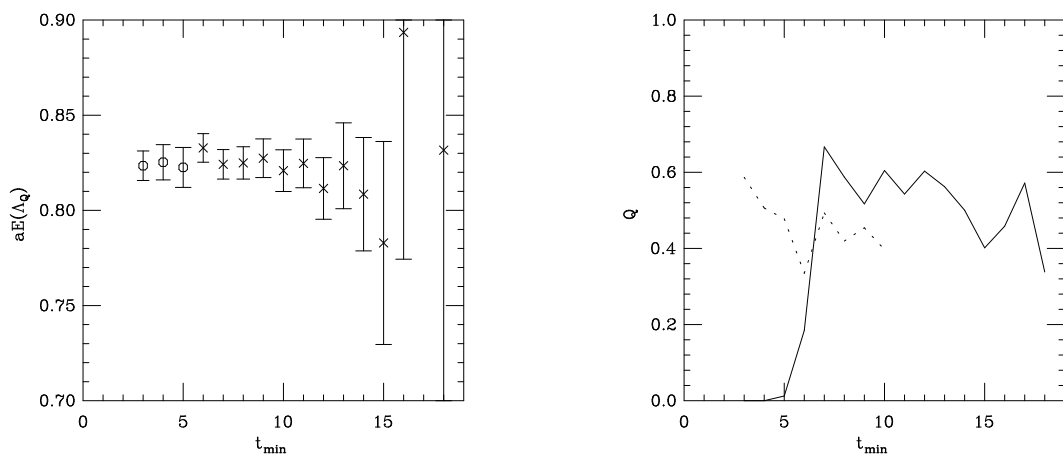


FIG. 14. The ground state energy of the  $\Lambda_Q$  extracted from a  $n_{exp} = 1$  (crosses) and  $n_{exp} = 2$  (circles) fit to the  $C(l, 1)$  correlator as a function of  $t_{min}$  for  $aM_0 = 1.0$  and  $\kappa_l = 0.1385$ ;  $t_{max} = 20$ . The corresponding values of  $Q$  are also shown as a solid (dotted) line for a  $n_{exp} = 1$  (2) fit.

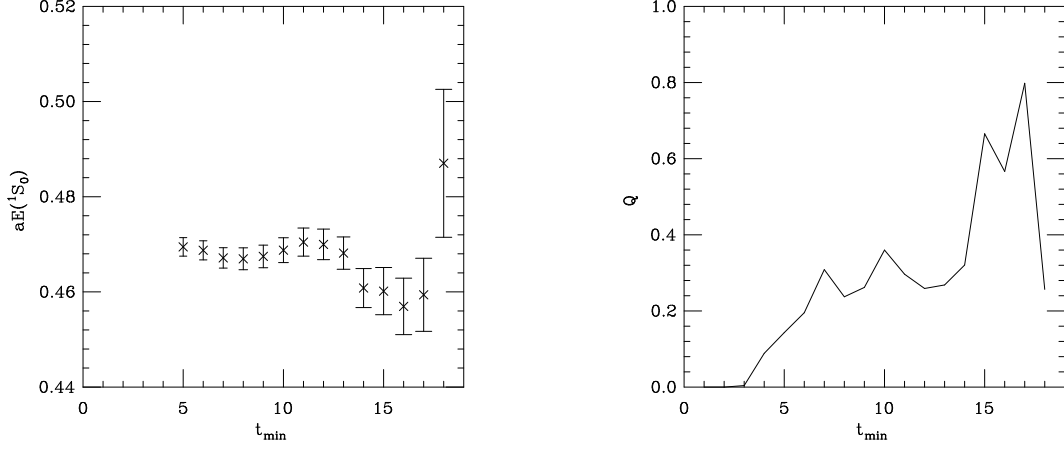


FIG. 15. The ground state energy extracted from a  $n_{exp} = 1$  fit to the pseudoscalar  $C(l, 1)$  and  $C(1, 1)$  meson correlators as a function of  $t_{min}$  for  $aM_0 = 1.0$  and  $\kappa_l = 0.1385$ ;  $t_{max} = 20$ . The corresponding values of  $Q$  are also shown.

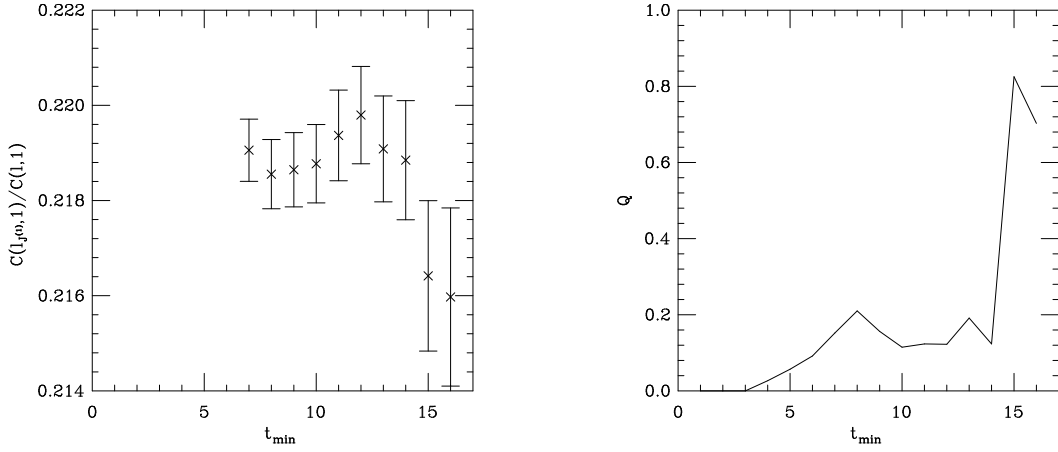


FIG. 16. The ratio  $C(l_{J(1)}, 1)/C(l, 1)$  for the  $PS$  meson as a function of  $t_{min}$  for  $aM_0 = 1.0$  and  $\kappa_l = 0.1385$ ;  $t_{max} = 20$ .